# 國 立 交 通 大 學

應 用 化 學 系 碩 士 班

碩　士　論　文

利用拉曼顯微光譜技術與成像法觀測在分子層級下活體的分裂酵母之細胞活性

*In Vivo* Molecular-Level Investigation of Cellular Activities of Fission Yeast Using Raman Microspectroscopy and Imaging

研究生：邱郁芳

指導教授:重藤真介 博士

中華民國一百年七月

# 利用拉曼顯微光譜技術與成像法觀測在分子層級下活體的分裂酵母之細胞活性

研究生：邱郁芳　　Student: Yu-Fang Chiu

指導教授：重藤真介 博士　　Advisor: Dr. Shinsuke Shigeto

國 立 交 通 大 學

應用化學系碩士班

碩 士 論 文

A Thesis Submitted to M. S. Program, Department of Applied Chemistry
College of Science
National Chiao Tung University
in part Fulfillment of the Requirements
for the degree of
Master
in
M. S. Program, Department of Applied Chemistry

July 2011

Hsinchu, Taiwan, Republic of China

中華民國一百年七月

# 利用拉曼顯微光譜技術與成像法觀測在分子層級下活體的分裂酵母之細胞活性

學生: 邱郁芳　　指導教授:重藤真介 博士

國立交通大學應用化學系碩士班

## 摘要

此篇論文從許多會影響分裂酵母菌的細胞活性的因素中，針對酵母菌生長的溫度與其在細胞生長曲線中所處的成長階段作為探討的主軸，並且利用拉曼顯微光譜技術與成像法深入探討分裂酵母菌在分子層級下的活體生物活性。首先，我們探討 1602 $cm^{-1}$ 的拉曼訊號在各種溫度下訊號強度的變化，由文獻得知，1602 $cm^{-1}$ 的拉曼訊號的強度和酵母菌的代謝活性是息息相關的。而我們的結果顯示，酵母菌的 1602 $cm^{-1}$ 的拉曼訊號在 32 ℃的環境中，會達到最高值，而後此訊號隨著溫度上升逐漸地下降。在 35 ℃時，降幅達到最大值約 45%。但當培養環境超過 35 ℃時，1602 $cm^{-1}$ 的拉曼訊號將不再下降。此處 1602 $cm^{-1}$ 的拉曼訊號的在高溫的培養環境中逐漸地下降，代表著分裂酵母菌在高溫下具有較低的細胞活性。接著，我們利用拉曼光譜成像法探討分裂酵母菌在對數生長期與穩定生長期兩種不同生長階段時，生物分子在細胞中的分佈與組成的變化。實驗結果顯示，

在穩定生長期時，酵母菌中的磷脂質和蛋白質生物分子是區域化分佈於酵母菌的兩端。然而，在對數生長期時，磷脂質和蛋白質生物分子的分佈卻呈現均勻分佈於整個酵母菌。對於此生物分子組成的變化，我們認為也許是和酵母菌的能量儲存作用相關。因為在穩定生長期時，酵母菌會將磷脂質區域化於細胞的兩端，以利於能量的儲存。然而，對數生長期中的酵母菌是處於快速分裂且不斷生長的狀態，生產出的蛋白質和脂質大部分馬上被當作複製 DNA 的成分來源，所以它們不需要像在穩定生長期一樣被大量儲存。是故拉曼光譜影像顯示，對數生長期中的酵母菌並不具有明顯地脂質區域化分佈。

# *In vivo* Molecular-Level Investigation of Cellular Activities of Fission Yeast Using Raman Microspectroscopy and Imaging

Student: Yu-Fang Chiu Advisor: Dr. Shinsuke Shigeto

M. S. Program, Department of Applied Chemistry
National Chiao Tung University

## Abstract (in English)

A number of physiological parameters and conditions profoundly influence the bioactivity of cells in various ways. Here, among these parameters and conditions, we investigated the effects of growth temperature and phase of the growth curve on the cellular activities of *Schizosaccharomyces pombe* by using Raman microspectroscopy and imaging, *in vivo* and at the molecular level. First, in the study of the temperature effects on yeast Raman spectra, we focus on the variation of the intensity of the band at 1602 $cm^{-1}$, which is a Raman band that is highly relevant to metabolic activities of the yeast cells. The result shows that at ~32 ℃, the intensity of the 1602 $cm^{-1}$ band begins to decrease gradually by approximately 45% and seems to reach a plateau above ~ 35 ℃. This decrease in the 1602 $cm^{-1}$ band intensity is indicative of lowered metabolic activity of the yeast cells at such high temperatures. Second, Raman imaging was performed on *S. pombe* cells in different growth phases, *i.e.*, log and stationary phases, in order to examine how these growth phases affect molecular compositions and distributions in *S. pombe* cells. The observed Raman images revealed that the distributions of phospholipids and proteins are usually localized at the two sides of yeast cells in the stationary phase, while in the log phase, they appear to be more uniformly distributed over the whole cell. We interpret the localization of lipids in the stationary phase in terms of substantial energy storage in some particular regions of *S. pombe* cells. Compared with the stationary phase, the produced proteins and phospholipids may be consumed immediately for DNA duplication and other events, there may be no need for them to be stored in a large amount in the log phase. As a result, the cells do not show lipid localization as evidently as those in the stationary phase.

# Acknowledgments

屬於學生生涯的最後兩年結束了，今天我要畢業了!首先我要感謝當然是我的把拔、媽咪，他們給予我精神上的支持和鼓勵，以及提供我經濟上的幫助，讓我可以心無旁騖的完成我的學業，在桃園工作的老哥也會不時帶著伴手禮跑來新竹關心我這位老妹，讓我即使身處異鄉，也能感受來自宜蘭老家滿出來的溫暖，好窩心!再來要感謝我在新竹最好的朋友同時也是最好的室友，小雞，從大學時起算起和他有六年的情份，我最愛和她哈拉聊天，同時她也最常當我吐苦水的對象，有她的陪伴，讓我在新竹生活超開心!她也常陪我跑步、打羽毛球，讓我身材不致於在碩班兩年變化的太誇張!接下來要感謝所有實驗室成員的陪伴，第一批當然是和我同甘共苦的其他同居同學，絲絲(塞塞)、洗息剛、辰文、許智航，就讀碩班期間，我們一起學習，同時也在遇到瓶頸時互相鼓勵對方，激勵彼此幫助大家往前進，其次，是帶我的博班學長們，小胖子學長，蘇先生、海先生，和已經離開的博士後小宗，很感謝他們細心的教導我做實驗，當我在實驗方面遇到瓶頸時給予我許多建議幫助我學習，最後還有學弟妹們，蘋果，小豬(小遠、山豬)，阿輔，阿慧，承翰，感謝他們在實驗室的陪伴，並且當我在學習過程當中遇到障礙時也給予我許多安慰和建議，讓我堅持下去更加努力!有了大家的陪伴，我在實驗室兩年過得很快樂!當然最最要感謝是我的指導教授重藤真介，教授他都不會去硬性規定我們的作息和實驗時間，讓我們可以按照自己的步調去完成我的學業，他的教導方針是循循善誘，讓我們對實驗內容了解更加透徹，當我們有不懂的地方，他也會非常有耐心的指導我們，最重要當然是他給了我一張畢業證書!

# Tables of Contents

Page

Abstract (in Chinese) ..... i

Abstract (in English) ..... iii

Acknowledgments ..... iv

Tables of Contents ..... v

List of Figures and Tables ..... vi

Chapter I General Introduction ..... 1

Chapter II Confocal Raman Microspectrometer ..... 7

II-1. Introduction ..... 8

II-2. Laboratory-built confocal Raman microspectrometer ..... 8

Chapter III Temperature Effects on Raman Spectra of Fission Yeast Cells ..... 13

III-1. Introduction ..... 14

III-2. Experimental methods ..... 14

III-3. Results and discussion ..... 15

Chapter IV *In vivo* Multimode Raman Imaging of Living Yeast Cells in Different Growth Phases ..... 23

IV-1. Introduction ..... 24

IV-2. Experimental methods ..... 24

IV-3. Results and discussion ..... 25

IV-3-1. The correlation between the 1602 $cm^{-1}$ band and the 982 and 714 $cm^{-1}$ bands from a viewpoint of growth phases ..... 25

IV-3-2. Space-resolved Raman spectra of living S. pombe cells in the log and stationary phase ..... 26

IV-3-3. Raman imaging of living *S. pombe* cells in the log and stationary phases .. 27

Chapter V Summary ..... 42

References ..... 44

# List of Figures and Tables

Page

Figure I-1. Typical yeast growth curve ..... 6

Figure II-1. Schematic of the laboratory-built confocal Raman microspectrometer. ..... 11

Figure II-2. Lateral (XY) resolution calibration of the laboratory-built confocal Raman microspectrometer..... 12

Figure II-3. Axial (Z) resolution calibration of the laboratory-built confocal Raman microspectrometer..... 12

Figure III-1. Growth curves of *S. pombe* cells cultured at 30 and 38 ℃. ..... 19

Figure III-2. Typical Raman spectrum of an optically trapped single *S. pombe* cell. ..... 19

Figure III-3. Raman spectra of *S. pombe* yeast cells in stationary phase at ten distinct temperatures. ..... 20

Figure III-4. Optical images of *S. pombe* yeast cells cultured at 26.1, 30.3, 33.8, and 38.3 ℃. ..... 21

Figure III-5. Average area intensity ratios of five Raman bands to the 1440 $cm^{-1}$ band versus temperature. ..... 21

Figure III-6. Average area intensity ratio of the 1602 $cm^{-1}$ band to the 1440 $cm^{-1}$ band versus temperature. ..... 22

Figure IV-1. Growth curves of the wild-type fission yeast cell and those with their nucleus/mitochondria labeled with GFP, cultured in PMLU medium at 30 ℃.... 31

Figure IV-2. Optical images of fission yeast cells in log phase and stationary phase. ..... 31

Figure IV-3. Raman spectra of granules inside fission yeast cells in the log and stationary phases at 30 ℃.. ..... 32

Figure IV-4. Space-resolved Raman spectra of a fission yeast cell in the log phase. ..... 33

Figure IV-5. Space-resolved Raman spectra of a fission yeast cell in the stationary phase. ... 34

Figure IV-6. Optical images of ten wild-type *S. pombe* cells in log and stationary phases and corresponding Raman images constructed for seven Raman bands. ..... 36

Figure IV-7. Optical images and GFP images of six *S. pombe* cells with their nucleus labeled with GFP in log and stationary phases and corresponding Raman images constructed for seven Raman bands..... 37

Figure IV-8. Optical images and GFP images of seven *S. pombe* cells with their

mitochondria labeled with GFP in log and stationary phases and corresponding Raman images constructed for seven Raman bands. ..... 38

Figure IV-9. Typical cell cycle of *S. pombe* ..... 39

Figure IV-10. Typical cross-sections of yeast cells with which to quantify the distribution pattern..... 39

Figure IV-11. Statistics on the distribution pattern of four Raman bands in the log and stationary phases.. ..... 40

Figure IV-12. Triacylglycerol formation in yeast via different pathways. ..... 41

Table III-1. Band assignments for Raman spectra of single living *S. pombe* cells. ..... 18

# Chapter I

# General Introduction

Cellular activities are significantly affected by a variety of physiological parameters and conditions, which include oxidative stress, nutrition conditions, growth temperature, pH, phases in the growth curve or cell-cycle stages, and so forth. Many studies have been devoted to investigating the effects of these parameters and conditions on cellular activities of yeast as a model system for higher organisms [1-19]. In the present work, we perform molecular-level studies of cellular activities of *Schizosaccharomyces pombe* with focus placed on the effects of the growth temperature and of different phases in its growth curve.

*S. pombe*, also called "fission yeast", was isolated from East African millet beer in 1890 and first described in 1893 [20]. *S. pombe* is a rod-shaped unicellular eukaryote. A *S. pombe* cell typically measures 3–4 μm in diameter and 7–14 μm in length. Like cells of higher organisms, *S. pombe* cells divide by medial fission. They grow rapidly and are easy to be handled in the laboratory. Therefore *S. pombe* is one of the most extensively studied model organisms in research fields ranging from genetics to biochemistry. Detailed studies of *S. pombe* cells are anticipated to provide a firm basis for understanding of cellular activities and ultimately of life at the molecular level.

The methodology that we use here to look at cellular activities of fission yeast cells is Raman microspectroscopy and imaging. Raman microspectroscopy bears many advantages. First, it is nondestructive and less invasive. Second, because it is a label-free technique unlike fluorescence microscopy, there is no need to introduce probe molecules to the target cell. This advantage enables us to do exploratory research in which unknown cellular components could be investigated. Third, the Raman method usually does not require complicated sample pretreatment. Most importantly, it provides detailed and otherwise unobtainable molecular specific information of the cell, as vibrational spectra are called molecular fingerprints. Although it has several drawbacks such as interference with autofluorescence and long acquisition time, Raman microspectroscopy has been used as a powerful tool for investigating many biochemical systems.

In the first project of the present study, we examine the effect of growth temperature on the cellular activity of fission yeast using the intensity of a Raman band located at 1602 $cm^{-1}$ as a marker band. This Raman band has been proven highly sensitive to the metabolic activity of yeast cells and hence called the "Raman spectroscopic signature of life" by Huang and co-workers [11, 12]. In their pioneering work, they performed a Raman mapping experiment of the fission yeast with mitochondria labeled with green fluorescent protein (GFP). There is much evidence accumulated that the 1602 $cm^{-1}$ band sharply reflects the metabolic activity of fission and budding yeast cells in various aspects:

(1) Addition of a respiration inhibitor, KCN, to the culture medium of fission yeast cells resulted in a rapid decrease and subsequent disappearance of the 1602 $cm^{-1}$ band. Concomitantly, the phospholipids Raman bands gradually changed from well-shaped peaks to broad, diffused features. This observation suggests that the respiration activity of the fission yeast is first inhibited by KCN and then the lowered metabolic activity in turn gradually deteriorates the double-membrane structure of the mitochondrion [12].

(2) The 1602 $cm^{-1}$ band is also observed for isolated mitochondria and has been shown to behave in a similar manner when the isolated mitochondria are treated with another respiration inhibitor, $NaN_3$ [21].

(3) The 1602 $cm^{-1}$ band has been found to correlate with a starving death process of budding yeast cells, in which the appearance of the so-called dancing body inside vacuoles of budding yeast cells lowers the metabolic activity of the yeast and eventually leads to cell death in a few hours [9].

(4) The behavior of the 1602 $cm^{-1}$ band has been studied under different nutrition conditions, atmospheric conditions, and the presence of oxidative stress. It is shown that the intensity of the 1602 $cm^{-1}$ band of a yeast cell in water increased by a factor of ~1.5, 1 h after addition of YE medium to water as a nutrient. The intensity of the 1602 $cm^{-1}$ band was strong when yeast cells were cultured under a $N_2/^{16}O_2$ ($O_2$ = 20%) atmosphere

but weak when cultured under 100% $O_2$ and 100% $N_2$ atmospheres, indicating that the cells seem to lose their metabolic activity under 100% $O_2$ and 100% $N_2$ atmospheres. No $^{18}O$ isotope shift was observed for the 1602 $cm^{-1}$ band when yeast cells were cultured under a $N_2/^{18}O_2$ ($^{18}O_2$ = 20%) atmosphere, confirming that the origin of the 1602 $cm^{-1}$ band is neither $O_2$ nor an oxygen-containing small molecule [10].

Unfortunately, the origin of the 1602 $cm^{-1}$ band has not yet been identified. Nevertheless, all these experimental results clearly show that the 1602 $cm^{-1}$ band is a reliable indicator of the metabolic activity of living yeast cells. Following the previous work, we anticipate that the intensity of this Raman band can also be used as a sensitive probe to study the effect of culturing temperature on the cellular metabolic activity. Empirically, the optimum temperature for culturing *S. pombe* yeast cells is known to be around 30 ℃. The main objective of the first project (Chapter III) is to provide molecular insight into this phenomenon from Raman microspectroscopy. Does the 1602 $cm^{-1}$ signature indeed depend on temperature? If so, what is the optimum temperature determined from a molecular viewpoint? These are the questions that we would like to address in the first part of this thesis.

The second part of the present study (Chapter IV) concerns the relation between Raman images of *S. pombe* cells and phases in yeast's growth curve. The growth curve is obtained by plotting the number density of biological cells as a function of time. The typical growth curve of yeast exhibits a sigmoid or S-shaped curve (see Figure I-1), which can be classified into four main phases: the lag phase, log (exponential) phase, stationary phase, and death phase. When yeast cells are inoculated into a fresh growth medium, they enter the initial growth phase, *i.e.*, the lag phase. During the lag phase, also referred to as an adaptation period, cells are biochemically active but not dividing. Cells activate their metabolic pathways to make enough essential nutrients and prepare for dividing in the upcoming log phase. Therefore the cell number at the lag phase remains relatively constant

compared to the log phase. Once the metabolic pathways are activated, cells begin DNA duplication and division. This is the onset of the second phase of growth called the log phase, in which the cell number increases exponentially. After a while, the growth rate slowly decreases due to the variation in environment (*e.g.*, limited nutrition available and high cell density), and the growth curve goes into the stationary phase. During the stationary phase, cell metabolism ceases, and the rapid division stops. When cells eventually run out of all nutrients in the medium, they come to the death phase and many of them begin to die [18].

We employ Raman microspectroscopy and imaging to study molecular compositions and distributions in yeast cells in different growth phases with their nuclei or mitochondria labeled with GFP. Because different growth phases show distinct characteristics of the metabolic activity (*e.g.*, growth rate and cell density), the compositions and distributions of major cellular components such as proteins and phospholipids are also expected to be quite different. We find that both optical images and space-resolved Raman spectra of *S. pombe* cells appear different between log phase and stationary phase. Our Raman imaging results reveal that, in the stationary phase, phospholipids and proteins appear to be localized at the two ends of the yeast cell. In sharp contrast, in the log phase, the distributions of the two cellular components exhibit quite different patterns which are spread more evenly over the entire cell. We successfully demonstrate that different growth phases of the yeast cell result in distinct molecular distributions. GFP labeling of the nuclei or mitochondria of the yeast cell facilitates comparison with the Raman images for assignment of the observed Raman bands. In addition, we can identify the cell-cycle phase of the fission yeast from the number of nuclei found in GFP images. The Raman imaging results are discussed in terms of energy storage in the yeast.

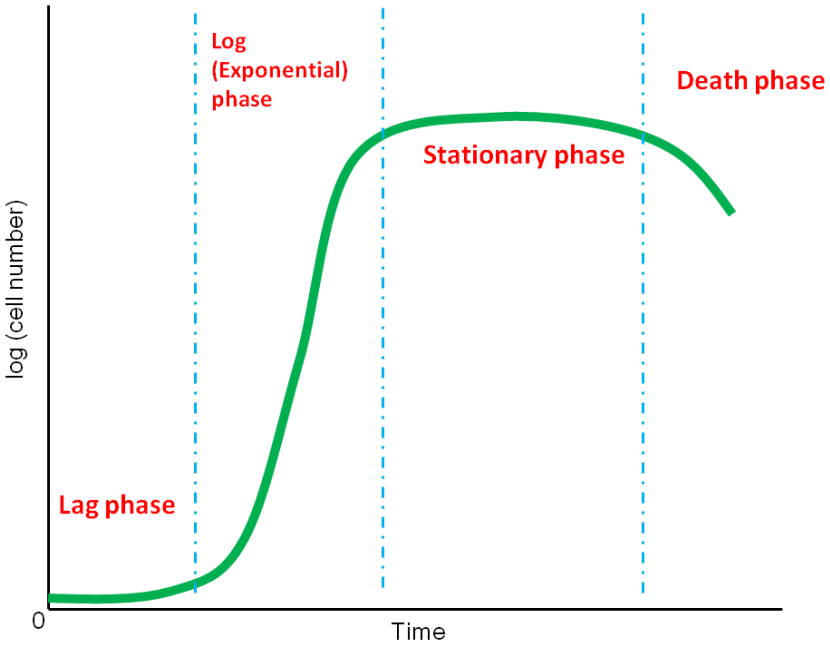


**Figure I-1.** Typical yeast growth curve, which consists of the lag, log (exponential), stationary, and death phases.

# Chapter II

# Confocal Raman Microspectrometer

## II-1. Introduction

Many of fundamental biological phenomena have been elucidated with the use of various biochemical methods. Nevertheless, most of the biochemical approaches lack time and space specificities and provide only time- and spaced-averaged molecular information. Raman microspectroscopy is a molecular microscopic technique with which time- and space-resolved information can be obtained. The method has several advantages such as being nondestructive and label-free, having high chemical specificity, and no complicated sample preparation required. Raman microspectroscopy has thus been widely used as a powerful tool for studying a multitude of biological samples including microorganisms, tissues, and plant and mammalian cells [6-8, 14, 22-38]. In this chapter, the laboratory-built confocal Raman microspectrometer used in the present study is described in detail.

## II-2. Laboratory-built confocal Raman microspectrometer

Figure II-1 is a schematic illustration of the laboratory-built confocal Raman microspectrometer [14, 31]. The 632.8 nm output of a He-Ne laser (Thorlabs) was used as the Raman excitation light. The laser beam was expanded by a factor of 2.67 in order to cover the exit pupil of the objective which we used. The expanded laser beam was introduced to a custom-made inverted microscope (Nikon; TE2000-U) by an edge filter (Semrock) and a hot mirror (Thorlabs). The laser beam was focused on the sample cell by an oil-immersion objective (CFI Plan Fluor; 100× oil, NA=1.3) placed on the microscope stage, and backward scattered light was collected by the same objective. The back-scattered light was guided along the opposite direction to the incoming path. The Rayleigh scattering and anti-Stokes Raman scattering were rejected with the edge filter and only Stokes Raman scattering was transmitted. Then the Stokes Raman scattered light was focused on a 100 μm pinhole by a 75 mm lens and then recollimated by another 75 mm lens. With the use of the 100 μm pinhole and the two 75 mm lenses for a confocal configuration, a spatial resolution of about 2.67(±0.05) μm in the axial (Z) direction was achieved. After the pinhole, the

Stokes Raman scattered light was introduced to a spectrometer (HORIBA Scientific; iHR320) and detected by a liquid nitrogen cooled charge-coupled device (CCD) detector (Princeton instruments; Spec-10:100) with 100 × 1340 pixels operating at −120 ℃. A 600 grooves/mm grating was used to cover a wide spectral range of >2000 $cm^{-1}$. For bright-field observation, the sample was illuminated by a halogen (or mercury) lamp and optical images were acquired by a digital camera (Nikon; DS-Ri1) equipped with the microscope. A set of excitation filter and emission filter (Semrock) were incorporated in the microscope for observation of fluorescence images of the cell whose organelles are labeled with GFP.

Figures II-2 and II-3 show the calibration results of the lateral (XY) and axial (Z) resolutions of our confocal Raman microspectrometer. To estimate the lateral resolution, we scanned horizontally a sharp edge of a silicon wafer using the intensity of the 520 $cm^{-1}$ band of silicon. For the axial direction, we measured the intensity rise of the 888 $cm^{-1}$ band of ethanol at an ethanol–glass interface. We made a plot of the Raman intensity versus scanned distance and fit the curve to Eq. II-1 [39].

$$f(x) = \frac{N}{2}\left(1 + \mathrm{erf}\left(\frac{x-a}{\sqrt{2}\sigma}\right)\right) + C \qquad \text{(II-1)}$$

where erf denotes the error function. The fitted results show that the spatial resolution was about 360(±4) nm in the lateral direction and 2.67(±0.05) μm in the axial direction. The uncertainties quoted here represent precisions in the fitting.

The laboratory-built confocal Raman microspectrometer can also be equipped with a 3-axis piezoelectric stage (PI; P-563.3CD) or a stage-top incubator (Tokai Hit; INU-ONICS-F1) on the microscope stage. The piezoelectric stage was used to perform Raman imaging experiments by translating the sample both horizontally and vertically. Sample scanning was controlled by a computer program based on LabVIEW (National Instruments). The stage-top incubator was employed to control the temperature of and

atmosphere around the medium by four independent heaters (stage heater, top heater, bath heater and lens heater) and by a gas-flow device, respectively. This device prevents the sample from drying, allowing us to perform longtime experiments.

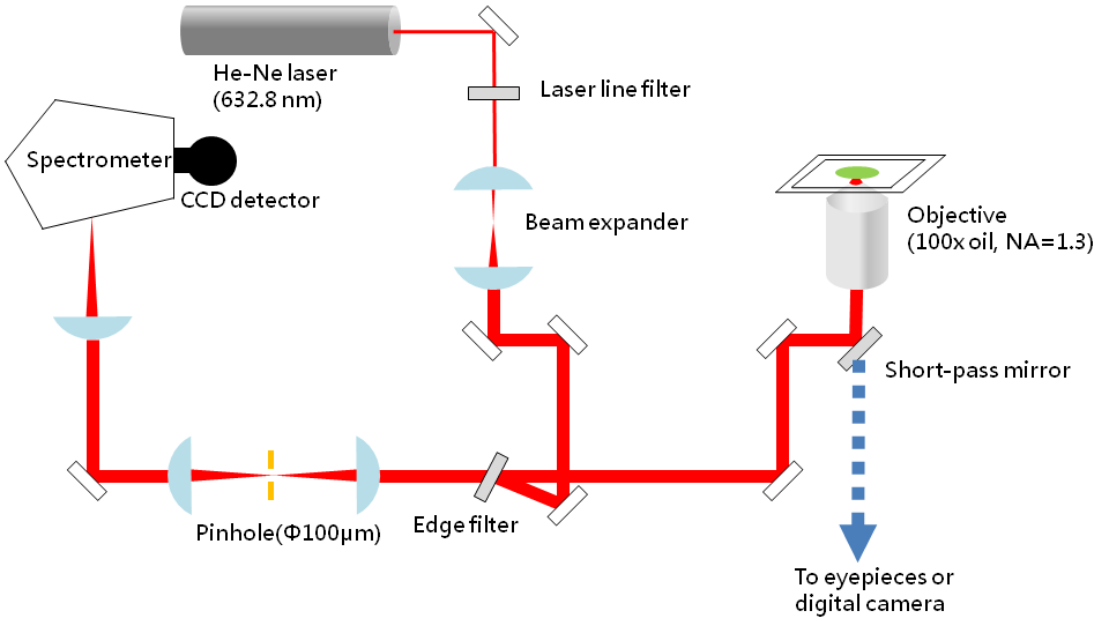


**Figure II-1.** Schematic of the laboratory-built confocal Raman microspectrometer.

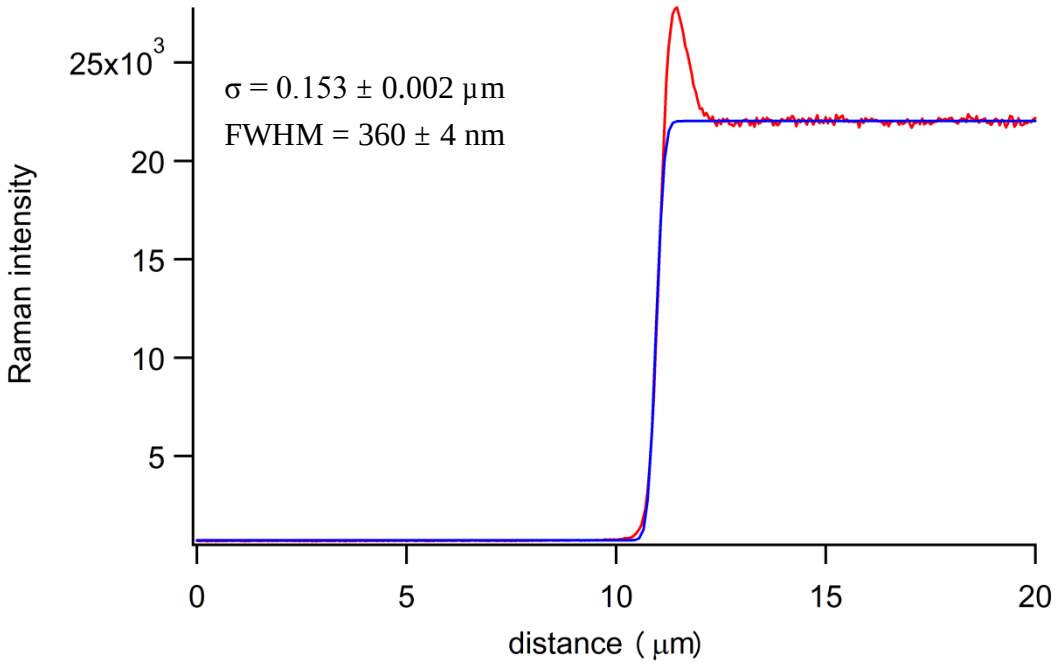


**Figure II-2.** Lateral (XY) resolution calibration of the laboratory-built confocal Raman microspectrometer. Red line, observed intensity change; blue line, best fit to the model function (Eq. II-1).

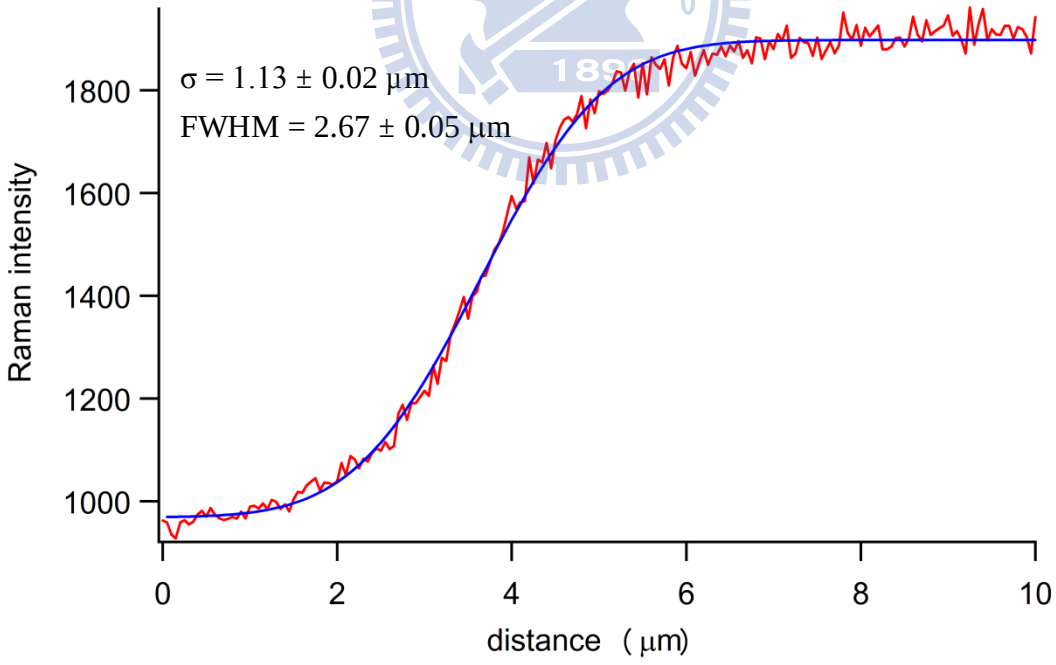


**Figure II-3.** Axial (Z) resolution calibration of the laboratory-built confocal Raman microspectrometer. Red line, observed intensity change; blue line, best fit to the model function (Eq. II-1).

# Chapter III

# Temperature Effects on Raman Spectra of Fission Yeast Cells

## III-1. Introduction

The effects of culturing temperature on Raman spectra of living fission yeast cells are investigated. The yeast cells are cultured at ten different temperatures ranging from 26 to 38 ℃, and their Raman spectra are recorded at these temperatures. First, we discuss major features of the observed Raman spectra of optically trapped yeast cells and the vibrational assignments of the Raman bands, which will also be of help for the next chapter. Next, we show the temperature dependence of the intensities of five representative Raman bands including the 1602 $cm^{-1}$ band, normalized by the intensity of the 1440 $cm^{-1}$ band (C–H bending). Interestingly, the intensity of the 1602 $cm^{-1}$ band drops by approximately 45% around 32–35 ℃, while those of the other bands remain nearly unchanged over the temperature range studied. This result strongly supports that the 1602 $cm^{-1}$ band serves as a sensitive probe of the metabolic activity of the yeast cells. However, no apparent maximum was found in the temperature dependence between 26 and 38 ℃.

## III-2. Experimental methods

In this measurement, we fix the growth period of the fission yeast to stationary phase. Yeast cells were cultured in YM medium (acumedia; 7363) in a shaking incubator at a given temperature (26.1, 28.4, 30.3, 31.7, 32.5, 33.8, 34.5, 35.5, 36.8, and 38.3 ℃) for 40 h in order for cells to reach stationary phase. Figure III-1 shows the growth curves of fission yeast cells cultured at 30 and 38 ℃, which were obtained by using a cell counting chamber (Marienfeld; 06 401 30). It is shown that after 40 h, cells can reach stationary phase even at 38 ℃, although the number of the yeast cells cultured at 38 ℃ is not as many as that at 30 ℃. Prior to Raman measurement, 1 mL of the medium was centrifuged and then the supernatant fluid containing the yeast cells was diluted in order to prevent from possible phase change and laser trapping of multiple cells. About 200 μL of the diluted medium was put on a glass bottom dish coated with poly-D-lysine (MatTek; P35G-1.5-14-C) for Raman measurement.

We set the measurement temperature to be the same as that for cell culturing by means

of the stage-top incubator mounted on the microscope stage. The target temperature was achieved by controlling the four heaters of the stage-top incubator. We estimated actual sample temperatures by measuring the temperature of water in the glass bottom dish inside the stage-top incubator with a thermometer (TENMARS; TM747D). We also input an air flow (~0.2 bar) into the stage-top incubator for every measurement. The 632.8 nm laser light was used for both excitation and trapping of the target cell. Optical trapping is a powerful technique with which to capture and manipulate biological particles at the focus of the laser beam for a long time. It permits optimum excitation and collection of Raman scattering in a confocal configuration [4, 40-42]. To avoid possible photobleaching and heat accumulation, the laser power was set to 2.6 mW at the sample point. A 60 s exposure time was used to measure the Raman spectra of optically trapped single yeast cells.

**III-3. Results and discussion**

Figure III-2 displays the typical Raman spectrum of an optically trapped fission yeast cell at 30 ℃ (both culture and measurement temperatures), which is the average spectrum of 30 different cells that were randomly chosen. As can be seen in Figure III-2, a number of characteristic Raman bands are observed in the so-called fingerprint region. Vibrational assignments of these bands have already been discussed in depth in the literature, which are summarized as follows. The 1744 $cm^{-1}$ band is assigned to the C=O stretch of the ester linkage [43]. The band at 1655 $cm^{-1}$ is due to the C=C stretch of the *cis* –CH=CH– linkage of unsaturated lipid chains. The strong 1440 $cm^{-1}$ band is ascribed to the C–H bending modes including $CH_2$ scissors and $CH_3$ degenerate deformation. The 1300 $cm^{-1}$ band is assigned to the in-phase $CH_2$ twisting mode. The band at 1266 $cm^{-1}$ is assigned to the C=C–H in-plane bend of the *cis* –CH=CH– linkage. Raman bands ascribable to carbohydrates are observed around 1030–1130 $cm^{-1}$ [35]. The bands at 1062 and 1122 $cm^{-1}$ are assigned to the out-of-phase and in-phase modes of the all-*trans* chain [44-46], while the band at 1082 $cm^{-1}$ is attributed to the *gauche* conformation. A Raman band due to the phospholipid headgroup is

observed around 715 $cm^{-1}$ [43]. The amide I mode may be responsible for the broad and weak feature that underlies the 1655 $cm^{-1}$ band. The CH bending modes of proteins may also overlap with the 1440 $cm^{-1}$ band. The bands at 1340 $cm^{-1}$ ($CH_2$ deformation) and 1266 $cm^{-1}$ (amide III), the broad band at 1154 $cm^{-1}$ (C–C and C–N stretching), and the sharp band at 1003 $cm^{-1}$ (phenylalanine residues) are ascribed to proteins. The "Raman spectroscopic signature of life", which is highly correlated to the metabolic activity of yeast cells, is observed at 1602 $cm^{-1}$ [11, 12]. These assignments can also be found as Table III-1.

Figure III-3 shows Raman spectra of optically trapped fission yeast cells in stationary phase grown at ten distinct temperatures. Each spectrum is the average of 30–50 spectra and has been normalized by the band area of the intense 1440 $cm^{-1}$ band (C–H bending mode). The use of the intensity of the 1440 $cm^{-1}$ band as a standard for normalization is justified by the fact that it has been found to remain almost constant over the whole temperature range. It is clearly seen that the 1602 $cm^{-1}$ band decreases in intensity at higher temperatures. In addition to spectral differences, in the course of yeast culturing, we also found that when the yeast cells are cultured at a higher temperature, the morphology of the cells looks quite different from yeast cells cultured at lower temperatures (see Figure III-4). There are more apparently dead cells found in the medium, suggesting that high-temperature environment somehow diminishes the yeast's cellular activities. How is such a temperature effect reflected in the intensities of representative Raman bands?

Figure III-5 shows the ratios of the average area intensity of five Raman bands (1655, 1602, 1300, 1003, and 718 $cm^{-1}$) to that of the 1440 $cm^{-1}$ band plotted as a function of temperature. The error bars in Figure III-5 represent standard deviations of 30–50 spectra used to calculate the average. The ratios for the bands at 1300 and 1003 $cm^{-1}$ show no particular tendency and seem to fluctuate with respect to the value at 26.1 ℃. The ratios for the 1655 and 718 $cm^{-1}$ appear to decrease slightly on going to higher temperature. In contrast, the 1602 $cm^{-1}$ band exhibits pronounced temperature dependence, in which the area intensity

ratio begins to drop at around 32 ℃, decrease by ~45%, and eventually reach a plateau above ~35 ℃. To better inspect the behavior of this Raman band, we re-plot its temperature dependence in Figure III-6. An approximately 45% decrease in the intensity of the 1602 $cm^{-1}$ band relative to that of the 1440 $cm^{-1}$ band is now more evident in this figure. It is definitely meaningful because it is larger than typical statistical errors.

Like previous studies, the 1602 $cm^{-1}$ band has again proven useful as a sensitive indicator of the cellular activity. The other bands ascribable to protein and/or phospholipid vibrations respond to temperature much less markedly than the 1602 $cm^{-1}$ band. As expected, culturing temperatures higher than 35 ℃ are presumably too severe for *S. pombe* cells to maintain the normal metabolic activity, although they are believed to be still alive based on the spectral pattern and optical image. It should be noted that we are unable to unambiguously determine the optimum temperature for culturing fission yeast from the temperature dependence shown in Figure III-6. It would be possible to argue that the ratios at 31.7 and 32.5 ℃ may be slightly higher than the others, but the apparent increase at these temperatures is comparable to the errors. Culturing conditions other than temperature could also affect the metabolic activity of *S. pombe*.

**Table III-1.** Band assignments for Raman spectra of single living *S. pombe* cells.

| Wavenumber ($cm^{-1}$) | Assignment |
|---|---|
| 715 | Phospholipid headgroup |
| 782 | RNA |
| 1003 | Phenylalanine residues |
| 1062 | Out-of-phase mode of the all-*trans* chain |
| 1082 | *Gauche* conformation |
| 1122 | In-phase mode of the all-*trans* chain |
| 1154 | C–C and C–N stretching |
| 1266 | C=C-H in-plane bend of the *cis*- –CH=CH– linkage and amide III |
| 1300 | In-phase $CH_2$ twisting mode |
| 1340 | $CH_2$ bending of the aliphatic chain |
| 1440 | $CH_2$ bending of the aliphatic chain |
| 1602 | "Raman Spectroscopic Signature of Life" [11, 12] |
| 1655 | *cis*- C=C stretch of unsaturated lipid chains and amide I mode |
| 1744 | C=O stretch of the ester linkage |

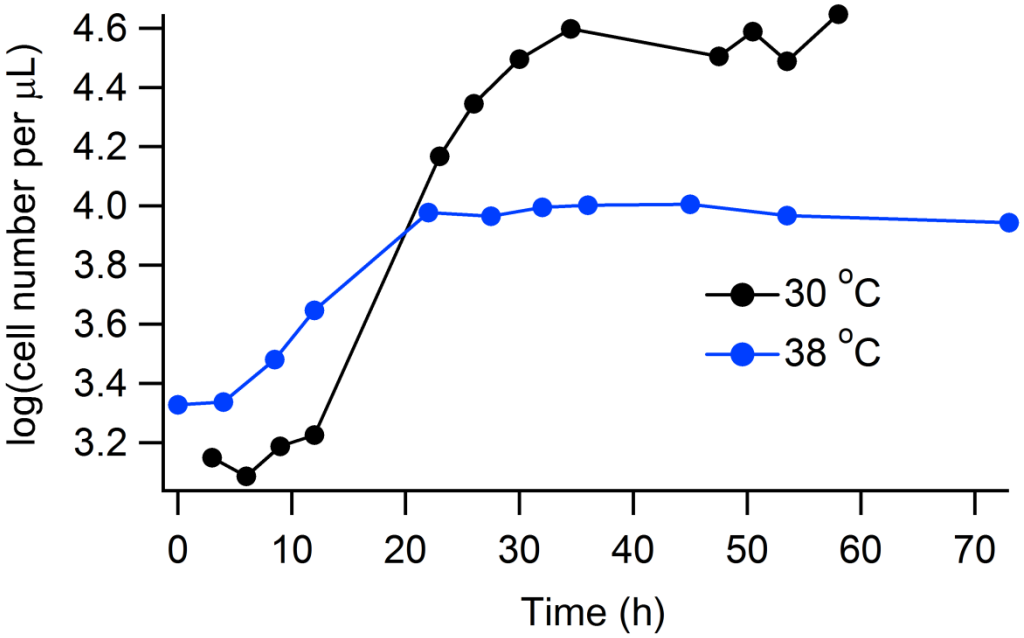


**Figure III-1.** Growth curves of *S. pombe* cells cultured at 30 and 38 ℃.

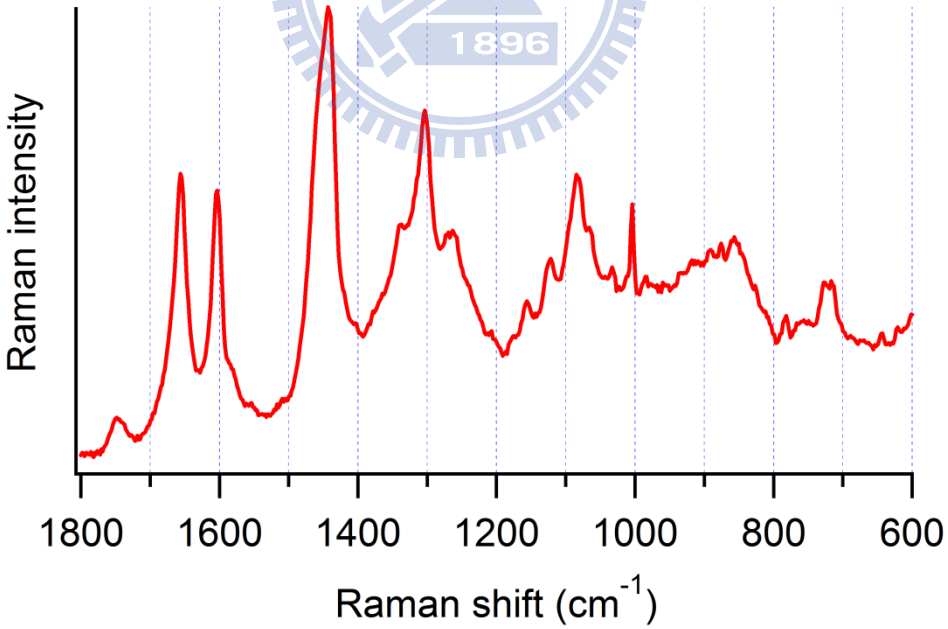


**Figure III-2.** Typical Raman spectrum of an optically trapped single *S. pombe* cell.

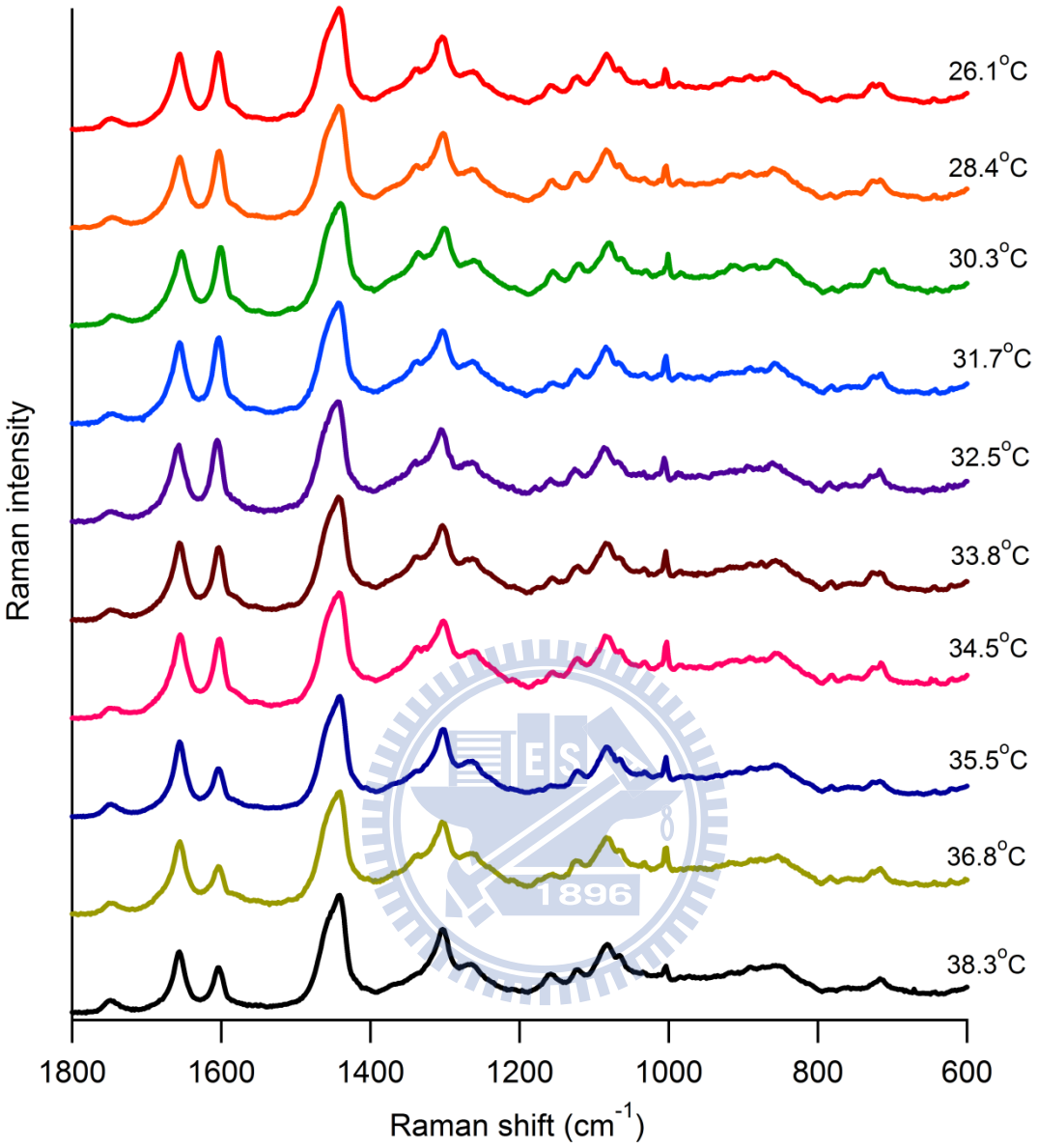


**Figure III-3.** Raman spectra of *S. pombe* yeast cells in stationary phase at ten distinct temperatures. Each spectrum is the average of 30–50 spectra and normalized by the area intensity of the 1440 $cm^{-1}$ band (C–H bending mode). Due to the lowered cell metabolic activity, the intensity of the 1602 $cm^{-1}$ band decreases at temperatures higher than ~35 ℃, while the change in other band intensities is not clear in this figure.

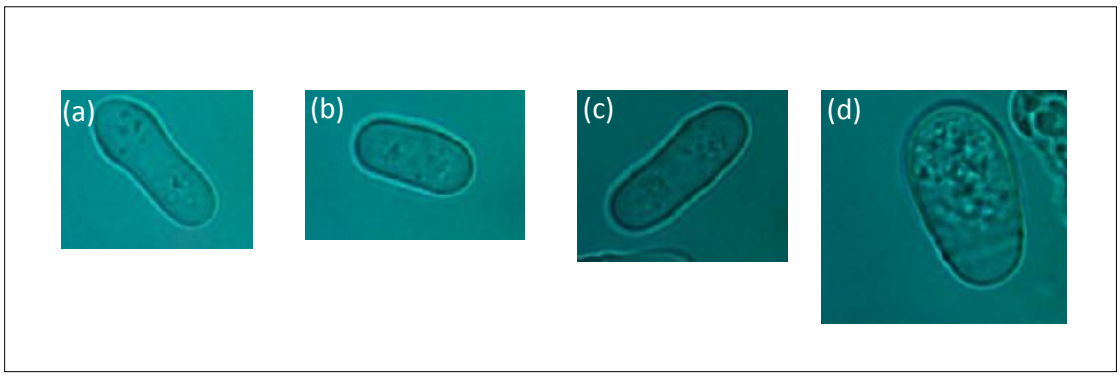


**Figure III-4.** Optical images of *S. pombe* yeast cells cultured at (a) 26.1, (b) 30.3, (c) 33.8, and (d) 38.3 ℃.

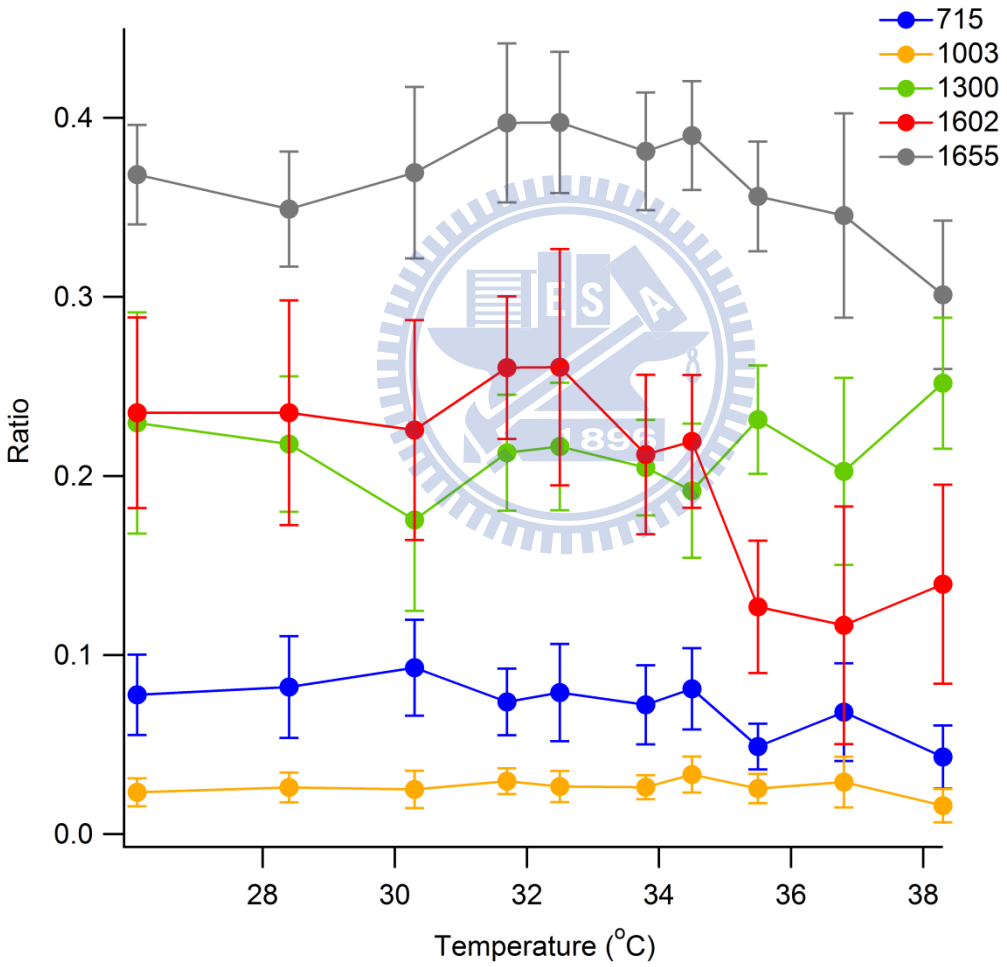


**Figure III-5.** Average area intensity ratios of five Raman bands to the 1440 $cm^{-1}$ band versus temperature. It is evident that the 1602 $cm^{-1}$ band shows the most marked decrease in intensity at high temperatures (>35 ℃).

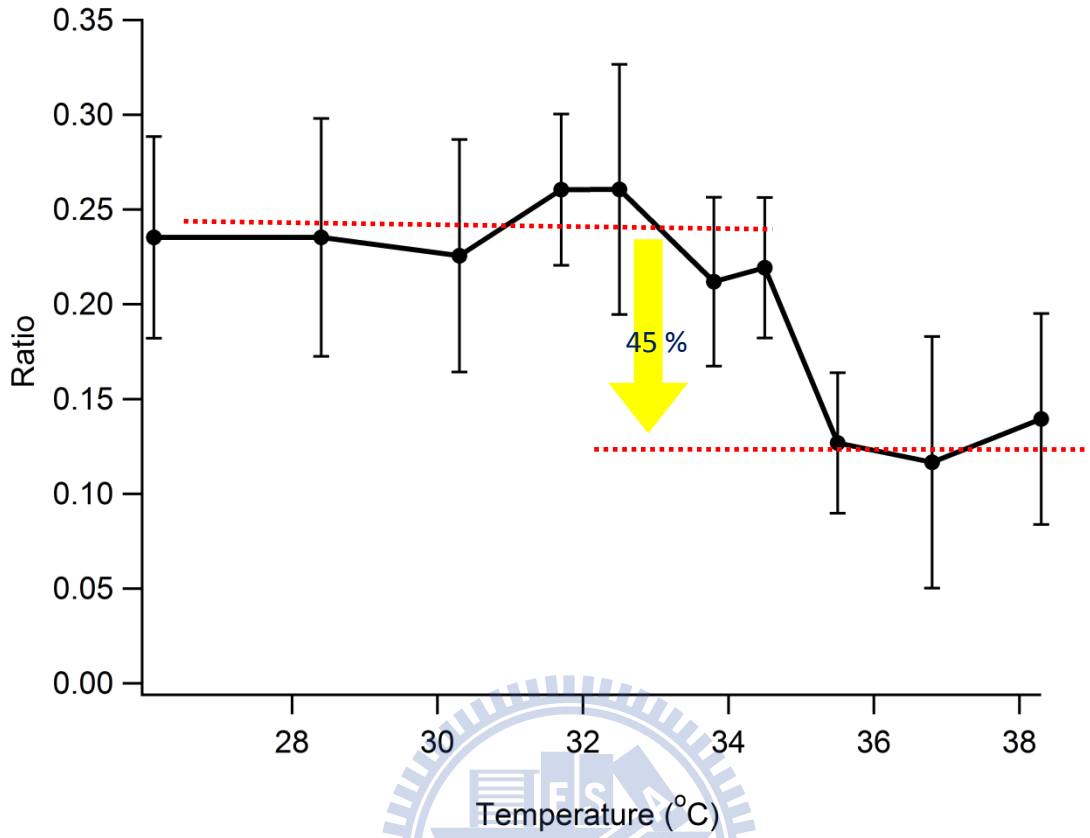


**Figure III-6.** Average area intensity ratio of the 1602 $cm^{-1}$ band to the 1440 $cm^{-1}$ band versus temperature. At ~32 ℃, the ratio begins to decrease gradually. It decreases by approximately 45% at ~35 ℃ and seems to reach a plateau above ~35 ℃. This decrease is most likely to be caused by the lowered metabolic activity of the cells at such high temperatures.

# Chapter IV

# *In vivo* Multimode Raman Imaging of Living Yeast Cells in Different Growth Phases

## IV-1. Introduction

Raman imaging experiments are performed for *S. pombe* cells in two different growth phases, namely, log and stationary phases. The observed Raman images reveal that the distributions of lipids and proteins are usually localized at the two ends of yeast cells in the stationary phase, while in the log phase, they appear to be more evenly distributed over the entire cell. We discuss this localization behavior of lipids in the stationary phase in relation to energy storage of *S. pombe* cells.

## IV-2. Experimental methods

In addition to the wild-type fission yeast, we used the cells with their nucleus/mitochondria labeled with GFP. These cells were immobilized on a glass-bottom dish coated with poly-D-lysine and cultured with PMLU ("Pombe Mineral Leucine Uracil") medium. Figure IV-1 displays the growth curves of the wild-type *S. pombe* cell as well as those with their nucleus/mitochondria labeled with GFP, cultured in PMLU medium. They all show similar patterns: namely, they reach the log and stationary phases at virtually the same time points.

Before reaching the log phase, yeast cells were cultured in PMLU medium overnight at 30 ℃, and then they were transferred onto a glass bottom dish and diluted with 200 μL of fresh PMLU medium. After dilution, the yeast entered the lag phase, and we continued culturing them at 30 ℃ for about 12 h until they reached the log phase. This sample was used for the log-phase experiment. For the stationary-phase experiment, yeast cells were cultured in PMLU medium at 30 ℃ for 40 h (see Figure IV-1). Prior to Raman imaging measurements, cells were put on a glass bottom dish, and 200 μL of the supernatant fluid was used to further dilute the cells to avoid possible variation in the growth phase.

For Raman imaging measurements, we employed the 3-axis piezoelectric stage mounted on the microscope stage to scan the target cell horizontally and to obtain the

information on the spatial distribution. The exposure time was 1 s at each point for Raman imaging measurements and 60 s for space-resolved measurements. The laser power was reduced to 2.6 mW at the sample point.

**IV-3. Results and discussion**

**IV-3-1. The correlation between the 1602 $cm^{-1}$ band and the 982 and 714 $cm^{-1}$ bands from a viewpoint of growth phases**

Figure IV-2 shows optical images of fission yeast cells in the log and stationary phases. The length of the yeast cells in the log phase are about 1.5 times longer than that in the stationary phase. Most of the cells are dividing in the log phase. In addition, there exist some granules (indicated by arrows) appearing as black spots inside the cells in both phases. In the log phase, granules are randomly distributed inside the cells, while in the stationary phase, they are mostly found at the two ends of each cell. Figure IV-3 compares the space-resolved Raman spectra recorded with the laser focused on granules in the log and stationary phases at 30 ℃. The Raman spectra are the average of 20–30 spectra and normalized with respect to the 1440 $cm^{-1}$ band. The major difference between the two spectra concerns three Raman bands at 1602, 982, and 714 $cm^{-1}$. In the log phase, the granule Raman spectrum shows the intense 1602 $cm^{-1}$ band, which is much stronger than the 1655 $cm^{-1}$ band, and accompanies the 982 $cm^{-1}$ band, which is as strong as the protein band at 1003 $cm^{-1}$. Furthermore, compared to the spectrum in the stationary phase, the 714 $cm^{-1}$ band is sharper in the log phase. A previous study by Onogi and Hamaguchi revealed that several Raman bands located in the 400–1200 $cm^{-1}$ interval as well as the 1602 $cm^{-1}$ band undergo photobleaching [47]. These Raman bands contain the 982 and 714 $cm^{-1}$ bands, which coincide with the Raman bands that are found in the present study to be stored in the log-phase spectrum.

The origin of the 1602 $cm^{-1}$ band has been discussed since its discovery. Very recently, ergosterol has emerged as one of plausible candidates as the origin. Ergosterol gives rise not

only to a band at 1602 $cm^{-1}$ but also bands at 714 and 982 $cm^{-1}$ [48]. Our data seem to agree with this working hypothesis and further indicate that the concentration of the molecular component inside the granules giving rise to the 1602 $cm^{-1}$ band varies between different growth phases. We also found that the variation of the intensity of the 982 $cm^{-1}$ band on going from the log to stationary phase correlates with that of the 1602 $cm^{-1}$ band. When the 1602 $cm^{-1}$ band is much stronger than the 1655 $cm^{-1}$ band (in the log phase), we can clearly see the 982 $cm^{-1}$ band, which is as strong as the 1003 $cm^{-1}$ band. However, when the 1602 $cm^{-1}$ band is weak and comparable in intensity to the 1655 $cm^{-1}$ band (in the stationary phase), the intensity of the 982 $cm^{-1}$ band is also weaker than the 1003 $cm^{-1}$ band. As for the 714 $cm^{-1}$ band, which is ascribed to the headgroup of phospholipids, is a broad band and usually appears as a doublet. A sharper form of the 714 $cm^{-1}$ band associated with stronger 1602 $cm^{-1}$ band in the log phase may be due to a higher concentration of the molecular component that gives rise to the 1602 $cm^{-1}$ band within the granules, possibly making one of the doublet peaks larger. We have also compared the area intensity of the 714 $cm^{-1}$ band in both phases and found that it is indeed larger in the log phase. The variation of the 714 $cm^{-1}$ band between the log and stationary phases involves not only intensity but also the band profile due probably to its multicomponent nature.

**IV-3-2. Space-resolved Raman spectra of living *S. pombe* cells in the log and stationary phase**

Figures IV-4 and IV-5 show the Raman spectra recorded at different locations in *S. pombe* cells in their log and stationary phases, respectively. Different from the spectrum of the granules, those space-resolved Raman spectra do not always an intense spectral signature at 1602 $cm^{-1}$. The general features seen from the space-resolved Raman spectra in the two phases can be summarized as follows. In the log phase, the Raman bands that give rise to both lipids and proteins (1655, 1440, and 714 $cm^{-1}$) and those that are assigned exclusively to lipids (1744 and 1300 $cm^{-1}$) are not strong. Instead, protein bands at 1340,

1154, and 1003 $cm^{-1}$ are more obvious. As opposed to the log phase, the spectra of the stationary phase show the strong 1602 $cm^{-1}$ band and lipid bands in most part of the cell except for the nucleus. As demonstrated by the space-resolved Raman spectra, the molecular composition changes from location to location within the yeast cell. Therefore, we decided to perform Raman imaging experiments in order to clarify how the major cellular components such as lipids and proteins distribute within the cell.

**IV-3-3. Raman imaging of living *S. pombe* cells in the log and stationary phases**

Figures IV-6–8 shows Raman images of seven Raman bands for the wild-type cells (Figure IV-6) and those with their nucleus (Figure IV-7) or mitochondria (Figure IV-8) labeled with GFP in log and stationary phases. The corresponding optical micrographs and GFP images are shown as well. All the GFP images in Figure IV-7 show a single nucleus, indicating that the cell is in the $G_2$ phase of the cell cycle. $G_2$ phase is one of the periods in the cell cycle. The cell cycle or cell-division cycle is one of the most fundamental biological processes, which consists of a series of events that take place in a cell for division and duplication. The typical cell cycle of *S. pombe* is depicted in Figure IV-9. *S. pombe* is known to have a very short $G_1$ phase, making it difficult to distinguish from the S phase. Therefore the notation $G_1$/S is used in the figure.

Seven Raman images in Figures IV-6–8 have been obtained simultaneously from each run of two-dimensional scan (multimode images). They have been normalized with respect to the intensity of the 1440 $cm^{-1}$ band so that we can compare the intensity distributions of a specific Raman band for different cells in the same color scale. We have chosen an appropriate color scale for each Raman band such that it can cover the whole range of the intensity distribution in different cells. However, some Raman bands are still so strong at some locations in the cells that the corresponding color is saturated. In such cases, we slightly modified the color scales so that the distribution inside the whole cell would be clearly discernible.

Except for the 1602 $cm^{-1}$ band, whose assignment is yet to be known, we classify other six Raman bands into three groups: the 1300 $cm^{-1}$ band originates from phospholipids (group 1); the 1340, 1154, and 1003 $cm^{-1}$ bands are assigned mainly to proteins (group 2); and the 1440 and 1655 $cm^{-1}$ bands are contributed by both phospholipids and proteins (and possibly other molecular components such as polysaccharides, group 3). First, we discuss characteristics of the intensity distribution patterns of the Raman images separately according to the above-mentioned classification.

- **Group 1: Phospholipid bands**

In the stationary phase, the intensity distribution of phospholipid bands evidently displays localized patterns around the two ends of each yeast cell. In the log phase, some of the yeast cells also show similar localized distributions but with a less contrast, namely, more uniformly distribution over the whole cell. The likelihood of highly localized patterns seems to be lower in the log phase than in the stationary phase.

- **Group 2: Protein bands**

The distribution of proteins is also shown to be highly localized at the two ends of the yeast in the stationary phase except for the 1003 $cm^{-1}$ band. For some stationary-phase yeast cells, the intensity distribution of the 1003 $cm^{-1}$ band does not represent definite patterns. This is partly because the 1003 $cm^{-1}$ band is a very sharp Raman band and can be buried under noises in the spectra. Consistent with the Raman images of group 1, in the log phase, the distribution of proteins is generally more uniform compared to that in the stationary phase. Additionally, we found that some of the yeast cells show extraordinary high intensities of the three protein bands in the log phase, which correspond to the protein-dominant spectra found in Figure IV-4.

- **Group 3: Phospholipid and protein bands**

A similar tendency to groups 1 and 2 is also found for group 3.

- **The 1602 $cm^{-1}$ band**

Compared to other phospholipid and protein bands, the intensity of the 1602 $cm^{-1}$ band is considerably affected by the cellular activity of each cell, resulting in relatively large individual variability. Nevertheless, we can conclude that the Raman image of the 1602 $cm^{-1}$ band tends to show a localized pattern at the two ends in the stationary phase, while in the log phase, it shows more or less uniform distributions.

To summarize, lipids, proteins, and the molecular component responsible for the 1602 $cm^{-1}$ band all show fairly localized distributions in both log and stationary phases, with a higher degree of localization found in the stationary phase.

To quantify whether a Raman image shows a localized or nonlocalized (uniform) pattern, we employ a preliminary analysis based on the intensity profile of a cross-section along the line connecting the central part of the cell. The way it works can be understood using Figure IV-10, in which representative cross-sections of two different cells for localized and nonlocalized cases are compared. To classify the Raman images as either localized or nonlocalized distribution, we calculate the value of *r*, using the following equations:

$$r = \frac{(I_a + I_b)/2 - I_c}{(I_a + I_b)/2 - (I_d + I_e)/2} \qquad \text{(IV-1)}$$

Here $I_a$, $I_b$, $I_c$, $I_d$, and $I_e$ represent the intensities at five characteristic points (a, b, c, d, and e) in the cross-section, respectively. If the ratio *r* for a Raman image is equal or greater than 0.30, we regard the distribution of this image as being localized; otherwise it is classified as being nonlocalized. The critical value of r = 0.3 has been chosen on the basis of a survey of many Raman images obtained in this study. Figure IV-11 shows the statistical results for the four images in the log and stationary phases at the Raman shift of 1440, 1300, 1154, and 1003 $cm^{-1}$. All studied cells ($N$ = 12) in the stationary phase (Figure IV-11b) are found to have a localized distribution pattern (*i.e.*, $r \geq 0.3$) with only one exception of the 1003 $cm^{-1}$ band due probably to lower signal-to-noise ratio. The tendency of localization of the

molecular components has thus been confirmed quantitatively. In the log phase (Figure IV-11a), however, the studied cells ($N$ = 19) show no definite tendency, and whether the Raman image has a localized pattern or not depends on the band. Proteins (1003 and 1154 $cm^{-1}$) are likely to be more uniformly distributed over the entire cell.

The high degree of lipid localization in the stationary phase may be interpreted in terms of energy storage of the cell. In stationary phase, cell division ceases and the growth rate becomes small (see Figure IV-1), so the cells tend to store energy under these circumstances. Phospholipids are known to be one of the essential components that convert diacylglycerol (DAG) to triacylglycerol (TAG) in TAG synthesis (Figure IV-12), which is associated with energy production of the cell [49, 50]. The localization of phospholipids in the stationary phase is thus possibly associated with energy storage in particular regions of the cell. In the log phase, the yeast cells are dividing rapidly and continuously, so the produced proteins and phospholipids may be immediately used as necessary components for DNA duplication and cell division. As a result, they are not accumulated in a large amount and do not show very sharp localization behavior compared to the results in the stationary phase.

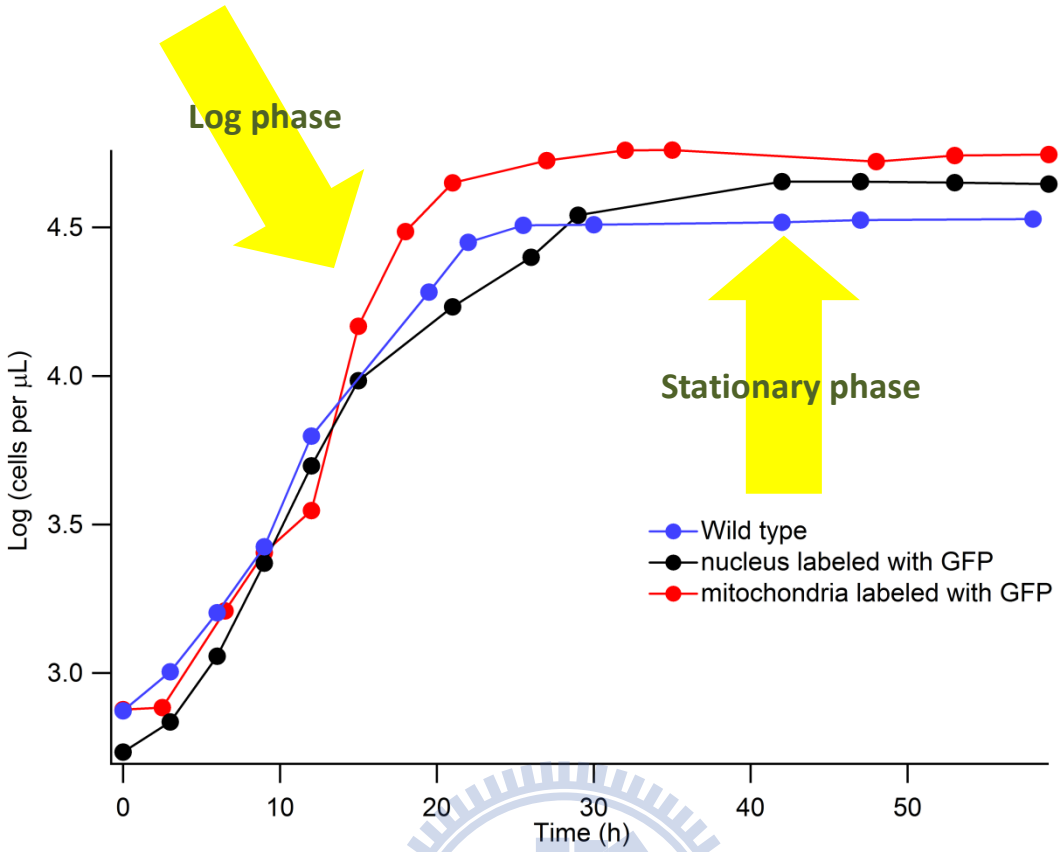


**Figure IV-1.** Growth curves of the wild-type fission yeast cell and those with their nucleus/mitochondria labeled with GFP, cultured in PMLU medium at 30 ℃.

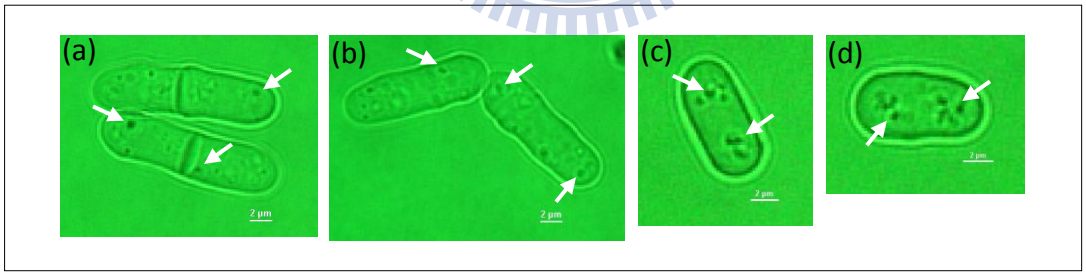


**Figure IV-2.** Optical images of fission yeast cells in log phase (a,b) and stationary phase (c,d). Arrows indicate several locations of granules (black spots).

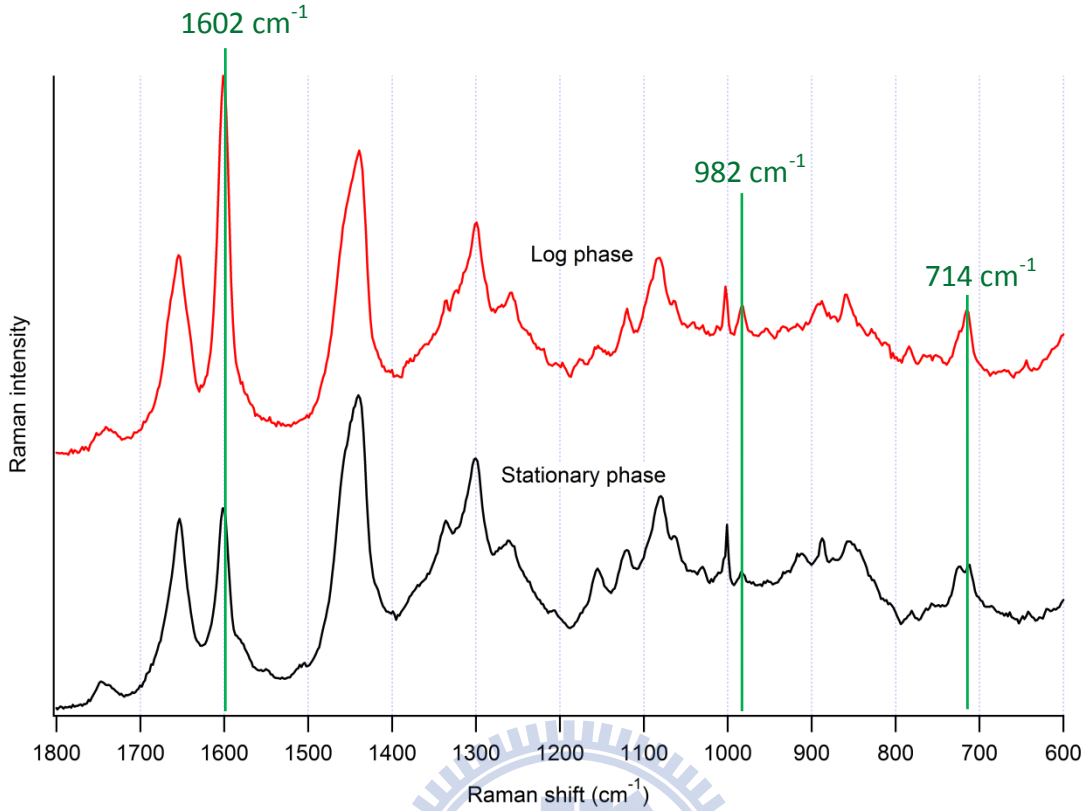


**Figure IV-3.** Raman spectra of granules inside fission yeast cells in the log and stationary phases at 30 ℃. Both spectra are the average of 20–30 spectra and normalized with respect to the 1440 $cm^{-1}$ band.

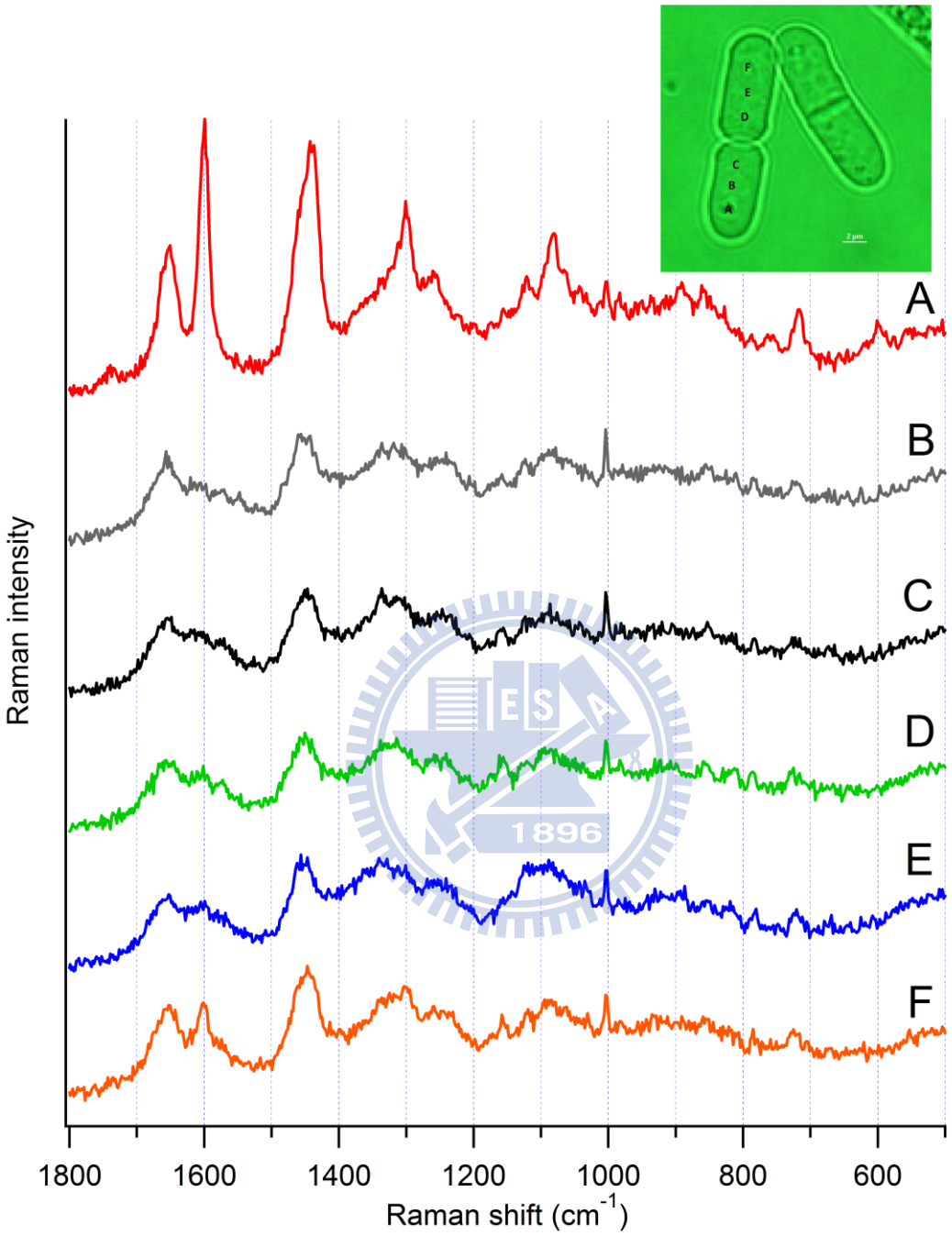


**Figure IV-4.** Space-resolved Raman spectra of a fission yeast cell in the log phase.

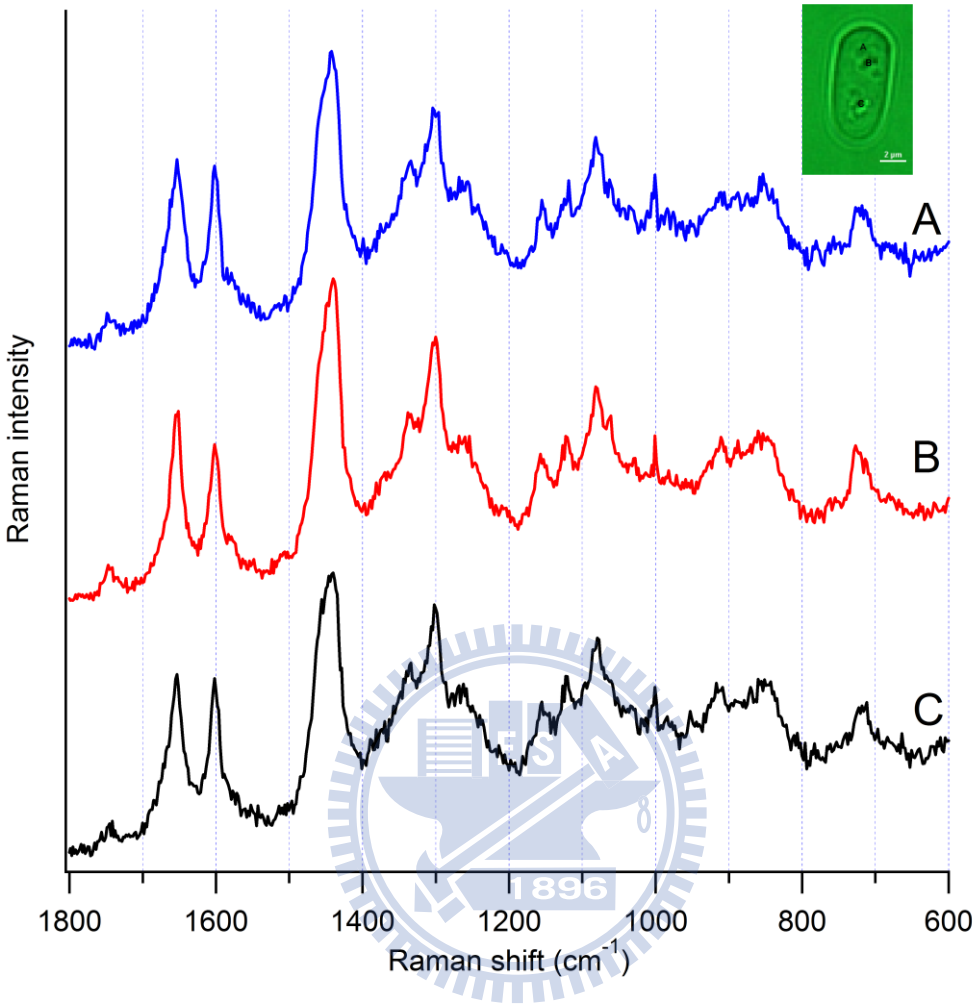


**Figure IV-5.** Space-resolved Raman spectra of a fission yeast cell in the stationary phase.

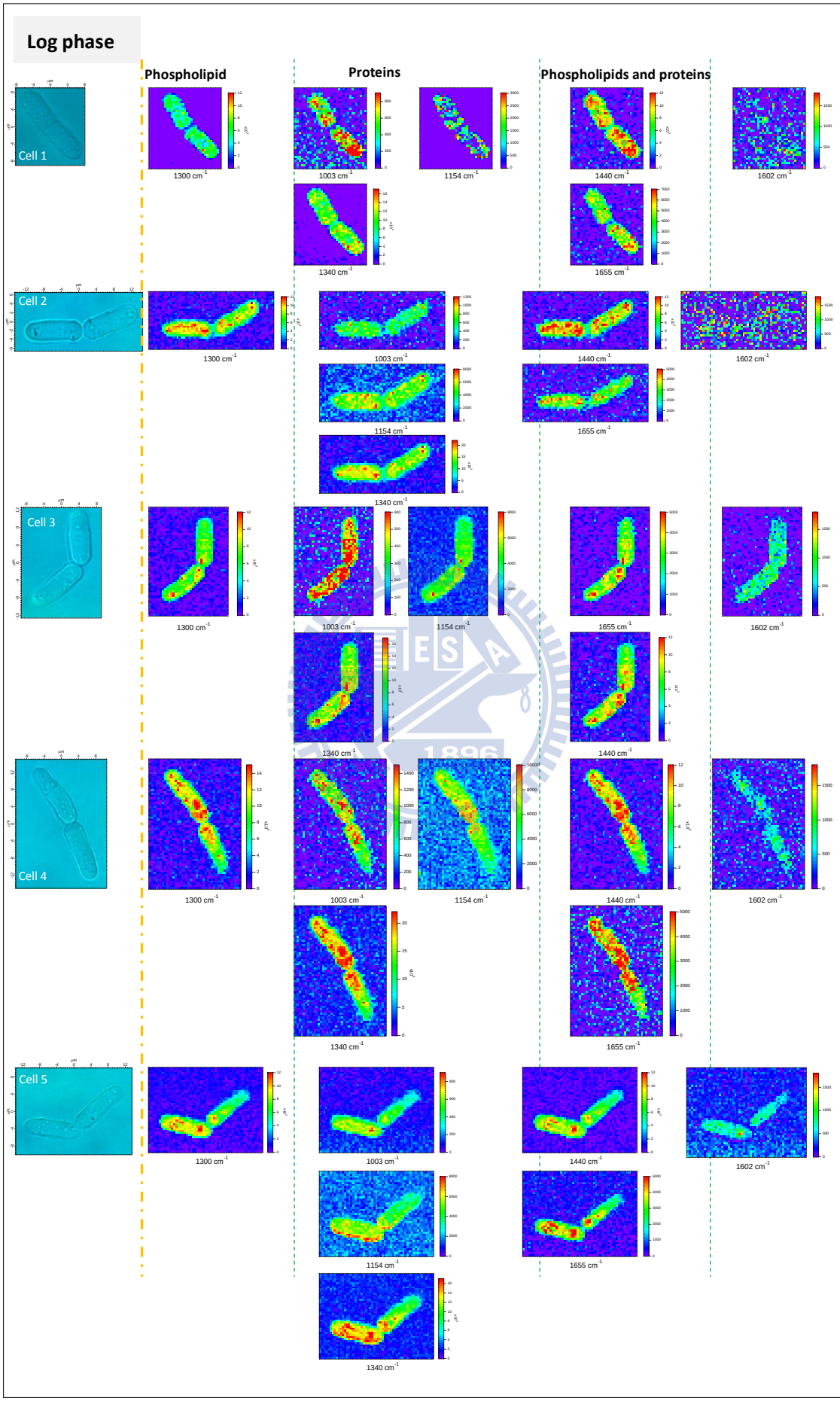
Log phase
Phospholipid
Proteins
Phospholipids and proteins
Cell 1
Cell 2
Cell 3
Cell 4
Cell 5
1300 cm-1
1003 cm-1
1154 cm-1
1340 cm-1
1440 cm-1
1655 cm-1
1602 cm-1

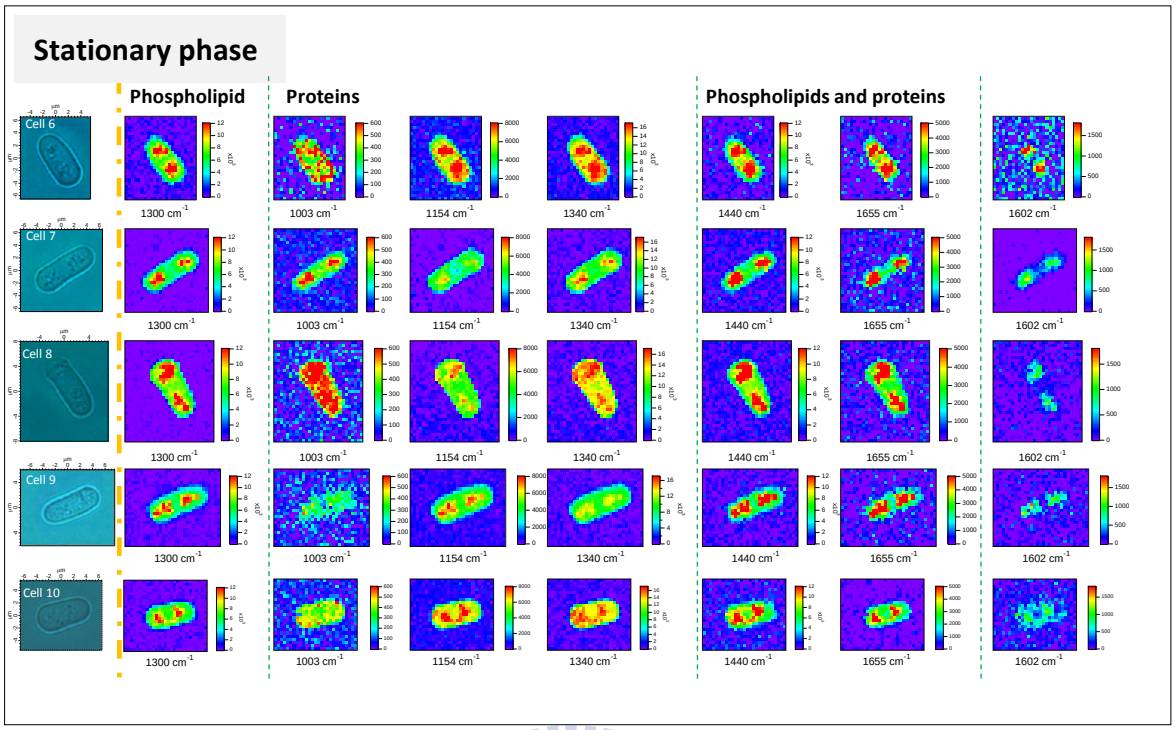


**Figure IV-6.** Optical images of ten wild-type (nonlabeled) *S. pombe* cells in log (first panel) and stationary (second panel) phases and corresponding Raman images constructed for seven Raman bands.

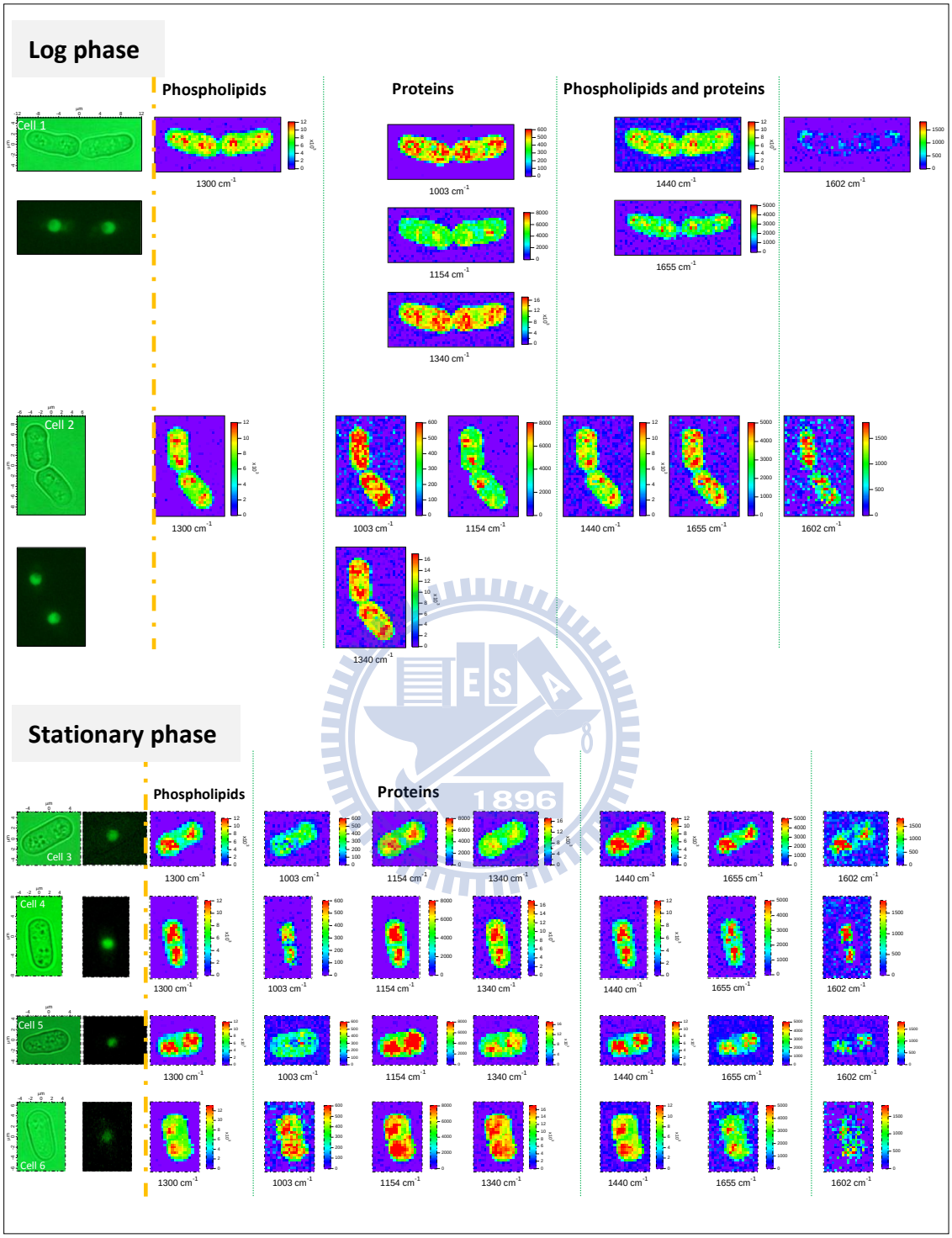


**Figure IV-7.** Optical images and GFP images of six *S. pombe* cells with their nucleus labeled with GFP in log (upper) and stationary (lower) phases and corresponding Raman images constructed for seven Raman bands. All cells are thought to be in the G2 phase of the cell cycle.

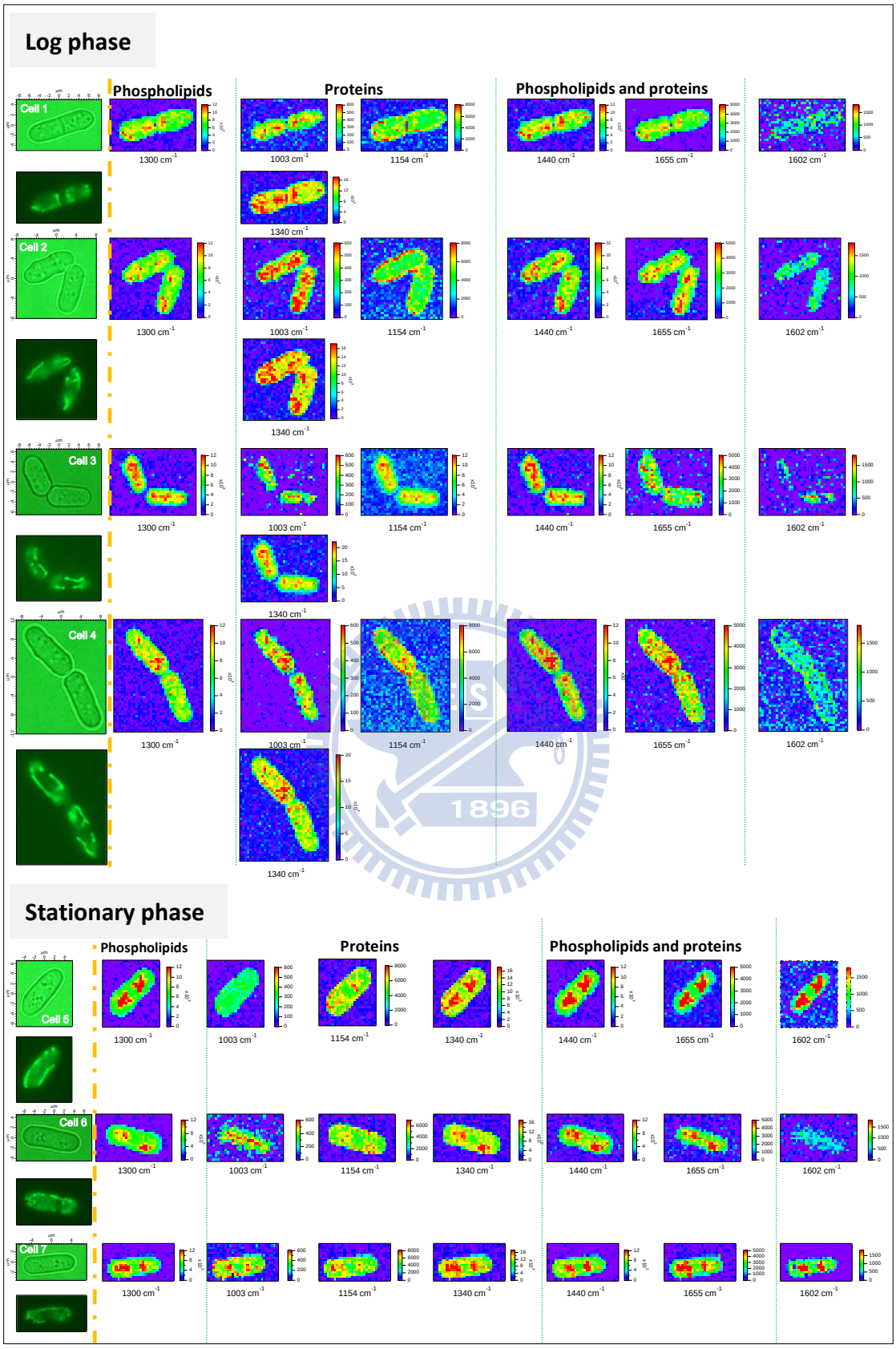


**Figure IV-8.** Optical images and GFP images of seven *S. pombe* cells with their mitochondria labeled with GFP in log (upper) and stationary (lower) phases and corresponding Raman images constructed for seven Raman bands.

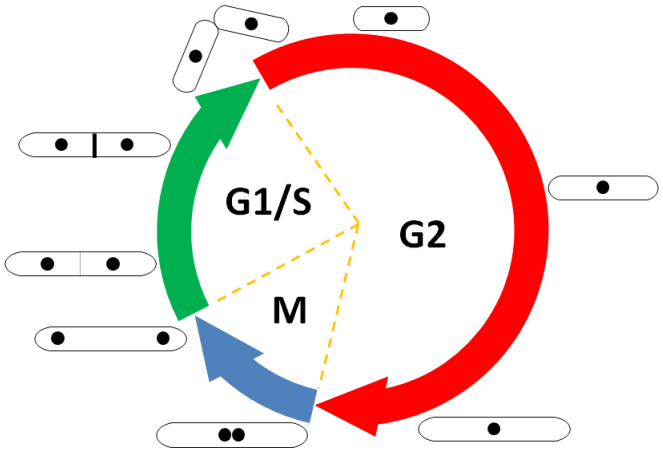


**Figure IV-9.** Typical cell cycle of *S. pombe*

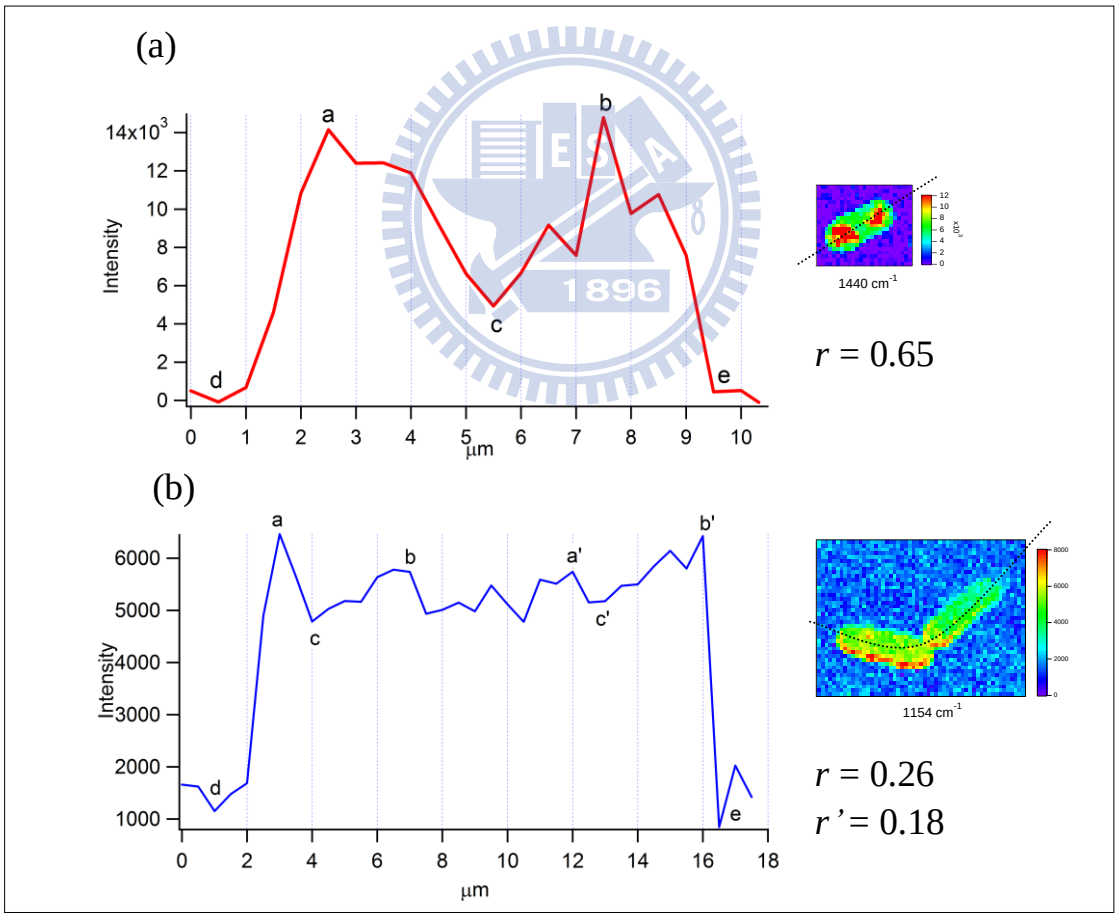


**Figure IV-10.** Typical cross-sections of yeast cells with which to quantify the distribution pattern. (a) Localized and (b) nonlocalized cases.

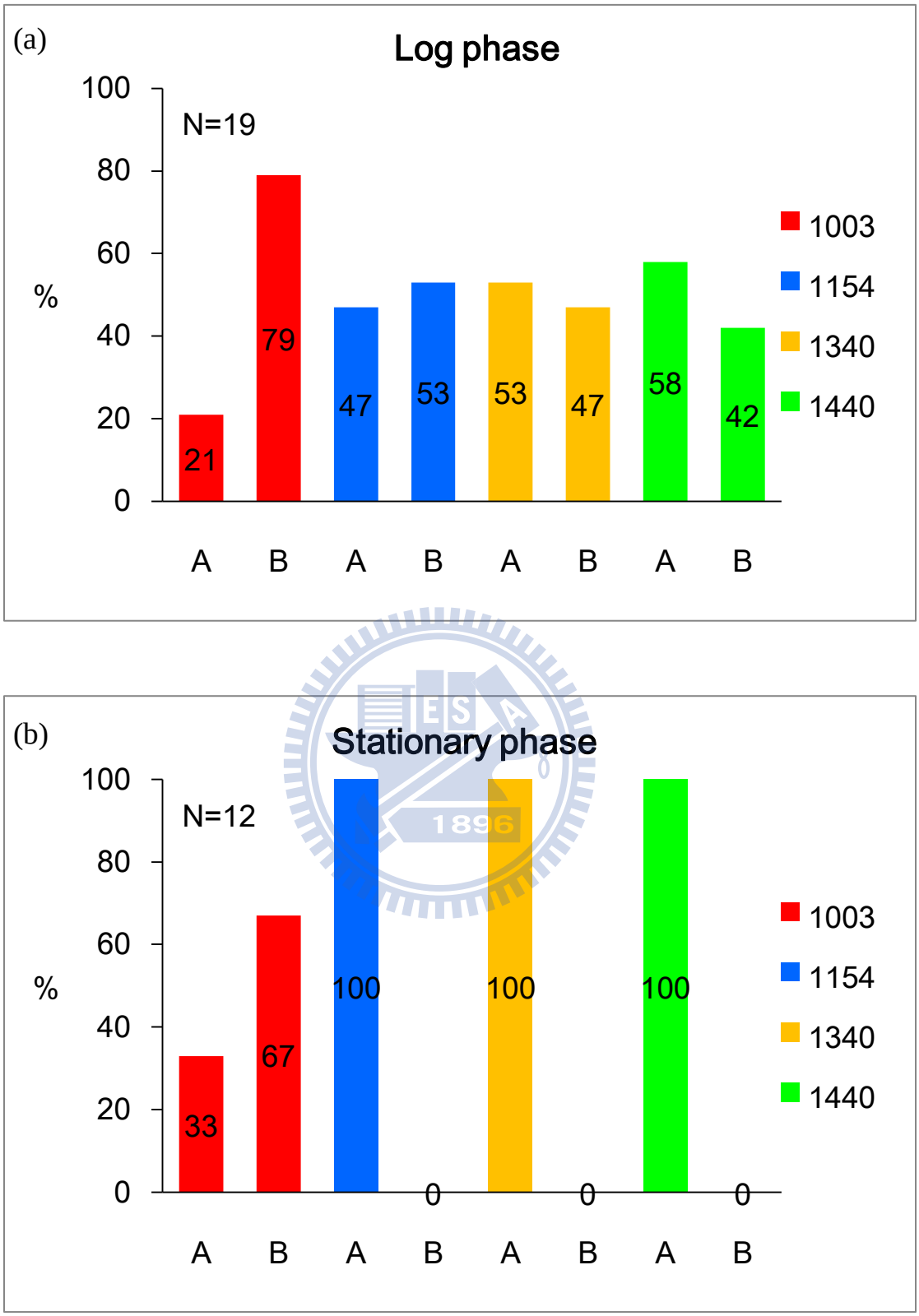


**Figure IV-11.** Statistics on the distribution pattern of four Raman bands in the log (a) and stationary (b) phases. A and B designate the localized and nonlocalized distribution, respectively, determined according to the ratio *r* [Eq. (IV-1)].

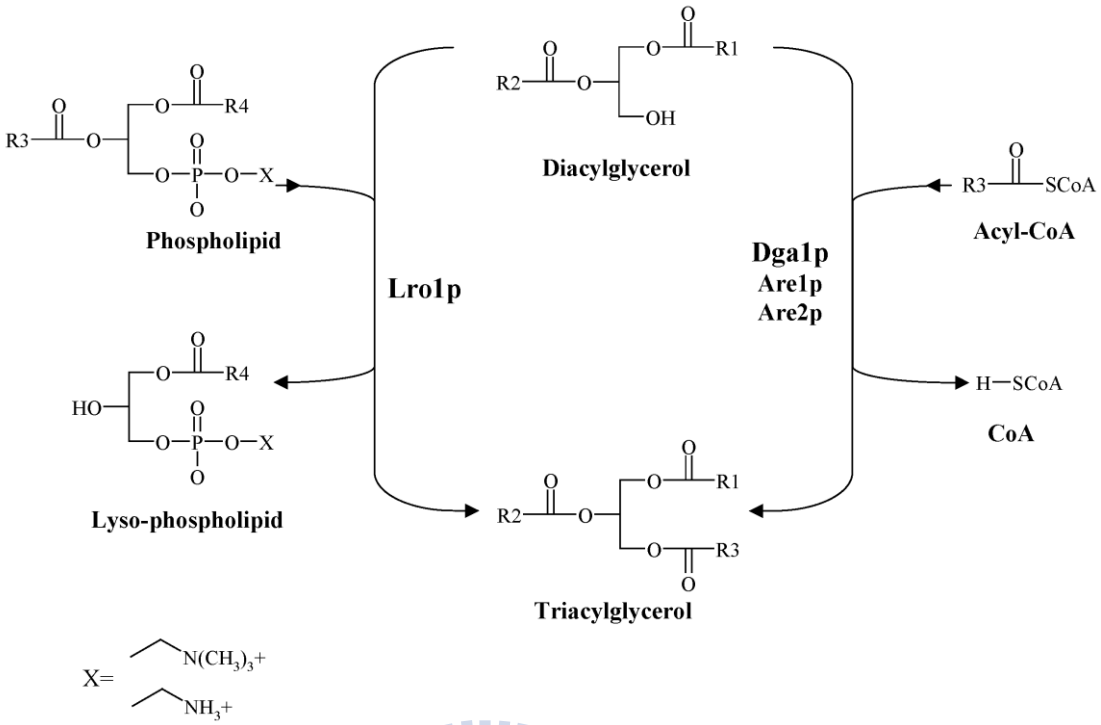


**Figure IV-12.** Triacylglycerol formation in yeast via different pathways (Taken from reference [49])

# Chapter V

# Summary

We used the intensity of the 1602 $cm^{-1}$ band, which was called the "Raman spectroscopic signature of life" by Hamaguchi and co-workers, as a sensitive probe to look into the effect of growth temperature on Raman spectra of fission yeast (*S. pombe*). We compared the average Raman spectra of 20–30 yeast cells cultured at ten distinct temperatures ranging from 26 to 38 ℃. It is found that the intensity of the 1602 $cm^{-1}$ band shows a decrease of about 45% at temperatures higher than ~32 ℃, although the intensities of other Raman bands remain almost constant with temperature. This result suggests that the metabolic activity of the cells is considerably lowered at such high temperatures.

Raman images of lipids and proteins in living *S. pombe* cells were compared between log and stationary phases in order to investigate the effect of different growth phases on the cellular activities. In the stationary phase, the distributions of both lipids and proteins are shown to be localized at the two ends of the cell. In the log phase, lipids and proteins appear to be distributed more evenly over the whole cell than in the stationary phase. This localization behavior observed particularly in the stationary phase may be relevant to substantial energy storage of the yeast cell. In contrast, the log-phase cells are usually dividing continuously, the produced proteins and phospholipids are used immediately as necessary components for DNA duplication and other cellular events, so that there might be no need for them to be stored.

## References


[1] D. Wawrzycka, *Postepy Hig Med Dosw,* vol. 65, pp. 328-337, Jun 2011.

[2] E. Swinnen, V. Wanke, J. Roosen, B. Smets, F. Dubouloz, I. Pedruzzi, E. Cameroni, C. De Virgilio, and J. Winderickx, *Cell Division,* vol. 1, p. 3, 2006.

[3] G. P. Singh, G. Volpe, C. M. Creely, H. Grötsch, I. M. Geli, and D. Petrov, *Journal of Raman Spectroscopy,* vol. 37, pp. 858-864, 2006.

[4] G. P. Singh, C. M. Creely, G. Volpe, H. G. tsch, and D. Petrov, *Analytical Chemistry,* vol. 77, pp. 2564-2568, 2005.

[5] P. Rösch, M. Harz, M. Schmitt, and J. Popp, *Journal of Raman Spectroscopy,* vol. 36, pp. 377-379, 2005.

[6] L. Peng, G. Wang, W. Liao, H. Yao, S. Huang, and Y. Q. Li, *Letters in Applied Microbiology,* vol. 51, pp. 632-638, 2010.

[7] C. Onogi, H. Torii, and H.-o. Hamaguchi, *Chemistry Letters,* vol. 38, pp. 898-899, 2009.

[8] C. Onogi and H.-o. Hamaguchi, *Chemistry Letters,* vol. 39, pp. 270-271, 2010.

[9] Y. Naito, A. Toh-e, and H.-o. Hamaguchi, *Journal of Raman Spectroscopy,* vol. 36, pp. 837-839, 2005.

[10] Y.-S. Huang, T. Nakatsuka, and H.-o. Hamaguchi, *Applied Spectroscopy,* vol. 61, pp. 1290-1294, 2007.

[11] Y.-S. Huang, T. Karashima, M. Yamamoto, T. Ogura, and H.-o. Hamaguchi, *Journal of Raman Spectroscopy,* vol. 35, pp. 525-526, 2004.

[12] Y.-S. Huang, T. Karashima, M. Yamamoto, and H.-o. Hamaguchi, *Biochemistry,* vol. 44, pp. 10009-10019, 2005.

[13] Y.-S. Huang, T. Karashima, M. Yamamoto, and H.-o. Hamaguchi, *Journal of Raman Spectroscopy,* vol. 34, pp. 1-3, 2003.

[14] C. K. Huang, H. O. Hamaguchi, and S. Shigeto, *Chem Commun (Camb),* Jul 20

2011.

[15] K. C. Chen, A. Csikasz-Nagy, B. Gyorffy, J. Val, B. Novak, and J. J. Tyson, *Molecular Biology of the Cell*, vol. 11, pp. 369-391, 2000.

[16] W.-T. Chang, H.-L. Lin, H.-C. Chen, Y.-M. Wu, W.-J. Chen, Y.-T. Lee, and I. Liau, *Journal of Raman Spectroscopy*, vol. 40, pp. 1194-1199, 2009.

[17] T. K. Bhowmick, G. Pyrgiotakis, K. Finton, A. K. Suresh, S. G. Kane, B. Moudgil, and J. R. Bellare, *Journal of Raman Spectroscopy*, vol. 39, pp. 1859-1868, 2008.

[18] M. Asaduzzaman, Master, Division of Mathematical Statistics and Department of Mathematical Sciences, Chalmers University of Technology and Göteborg University, Göteborg, Sweden, 2007.

[19] G. Aguirre-Alvarez, M. E. Rodriguez-Huezo, A. D. Hernandez-Fuentes, D. J. Pimentel-Gonzalez, and R. G. Campos-Montiel, *Journal of Animal Physiology and Animal Nutrition*, vol. 95, pp. 434-439, Aug 2011.

[20] P. von Lindner, *Wochenschr. Brau.*, vol. 10, pp. 1298-1300, 1893.

[21] L.-d. Chiu, M. Ando, and H.-o. Hamaguchi, *Journal of Raman Spectroscopy*, vol. 41, pp. 2-3, 2010.

[22] B. R. Wood, B. Tait, and D. McNaughton, *Biochimica et Biophysica Acta*, vol. 1539, pp. 58-70, 2001.

[23] H.-J. van Manen and C. Otto, *Journal of Raman Spectroscopy*, vol. 40, pp. 117-118, 2009.

[24] Y. Takai, T. Masuko, and H. Takeuchi, *Biochimica et Biophysica Acta*, vol. 1335, pp. 199–208, 1997.

[25] A. Sujith, T. Itoh, H. Abe, K.-i. Yoshida, M. S. Kiran, V. Biju, and M. Ishikawa, *Analytical and Bioanalytical Chemistry*, vol. 394, pp. 1803-1809, 2009.

[26] N. Stone, C. Kendall, J. Smith, P. Crow, and H. Barr, *Faraday Discussions*, vol. 126, p. 141, 2004.

[27] K. C. Schustera, E. Urlaubb, and J. R. Gapesa, *Journal of Microbiological Methods,* vol. 42, pp. 29-38, 2000.

[28] V. V. Pully and C. Otto, *Journal of Raman Spectroscopy,* vol. 40, pp. 473-475, 2009.

[29] C. Otto, N. M. Sijtsema, and J. Greve, *Eur Biophys J* vol. 27, pp. 582–589, 1998.

[30] C. Onogi, M. Motoyama, and H.-o. Hamaguchi, *Journal of Raman Spectroscopy,* vol. 39, pp. 555-556, 2008.

[31] H. N. Noothalapati Venkata, N. Nomura, and S. Shigeto, *Journal of Raman Spectroscopy,* pp. n/a-n/a, 2011.

[32] W. H. Nelson and J. F. Sperry, *Modern techniques for rapid microbiological analysis,* 1991

[33] W. H. Nelson, R. Manoharan, and J. F. Sperry, *Appl. Spectrosc. Rev.,* vol. 27, pp. 67-124, 1992.

[34] K. Maquelin, L.-P. i. Choo-Smith, T. v. Vreeswijk, H. P. Endtz, B. Smith, R. Bennett, H. A. Bruining, and G. J. Puppels, *Anal. Chem.* , vol. 72, pp. 12-19, 2000.

[35] J. L. Lippert and W. L. Peticolas, *Proc. Natl. Acad. Sci. U.S.A.,* vol. 68, pp. 1572-1576, 1971.

[36] K. De Gussem, P. Vandenabeele, A. Verbeken, and L. Moens, *Spectrochimica Acta Part A: Molecular and Biomolecular Spectroscopy,* vol. 61, pp. 2896-2908, 2005.

[37] L. P. Choo-Smith, H. G. M. Edwards, H. P. Endtz, J. M. Kros, F. Heule, H. Barr, J. S. Robinson, H. A. Bruining, and G. J. Puppels, *Biopolymers,* vol. 67, pp. 1-9, 2002.

[38] L.-d. Chiu and H.-o. Hamaguchi, *Journal of Biophotonics,* vol. 4, pp. 30-33, 2011.

[39] S. Ask, P. Barrillon, A. Braem, C. Cheiklali, I. Efthymiopoulos, D. Fournier, C. Delataille, B. Digirolamo, P. Grafstrom, and C. Joram, *Nuclear Instruments and Methods in Physics Research Section A: Accelerators, Spectrometers, Detectors and Associated Equipment,* vol. 568, pp. 588-600, 2006.

[40] C. Xie, C. Goodman, M. A. Dinno, and Y.-Q. Li, *Optics Express,* vol. 12, pp.

6208-6214, 2004.

[41] H. Tang, H. Yao, G. Wang, Y. Wang, Y.-q. Li, and M. Feng, *Optics Express*, vol. 15, pp. 12708-12716, 2007.

[42] D. G. Grier, *Nature*, vol. 424, pp. 810-816, Aug 2003.

[43] Y. Takai, T. Masuko, and H. Takeuchi, *Biochim. Biophys. Acta*, vol. 1335, pp. 199-208, 1997.

[44] M. Tasumi, T. Shimanouchi, and T. Miyazawa, *J. Mol. Spectrosc.*, vol. 9, pp. 261-287, 1962.

[45] R. G. Snyder and J. H. Schachtschneider, *Spectrochim. Acta*, vol. 19, pp. 85-116, 1963.

[46] R. G. Snyder, *J. Chem. Phys.*, vol. 47, pp. 1316-1360, 1967.

[47] C. Onogi and H.-o. Hamaguchi, *J. Phys. Chem. B*, vol. 113, pp. 10942–10945 2009.

[48] L.-d. Chiu, Ph. D Thesis, The University of Tokyo, 2011.

[49] D. Sorger and G. Daum, *Appl Microbiol Biotechnol*, vol. 61, pp. 289-299, 2003.

[50] H. Müllner and G. Daum, *Acta Biochemica Polonica*, vol. 51, pp. 323-347, 2004.